



**Deliverable 2.11: ILW: Report describing the
selected experiments and the existing/expected
experimental results**

Work Package **ACED**

The project leading to this application has received funding from the European Union's Horizon 2020 research and innovation programme under grant agreement No 847593.



<http://www.ejp-urad.eu/>

EURAD Deliverable 2.11 – ILW: Report describing the selected experiments and the existing/expected experimental results

Document information

Project Acronym	EURAD
Project Title	European Joint Programme on Radioactive Waste Management
Project Type	European Joint Programme (EJP)
EC grant agreement No.	847593
Project starting / end date	1st June 2019 – 30 May 2024
Work Package No.	WP2
Work Package Title	Assessment of Chemical Evolution of ILW and HLW Disposal Cells
Work Package Acronym	ACED
Deliverable No.	D2.11
Deliverable Title	ILW: Report describing the selected experiments and the existing/expected experimental results
Lead Beneficiary	ZAG
Contractual Delivery Date	December 2019
Actual Delivery Date	September 2020
Type	Report
Dissemination level	PU
Authors	Ana Mladenovic (ZAG), Erika Neeft (COVRA), Guido Deissmann (FZJ), Rainer Dähn, Guoqing Geng, Georg Kosakowski (PSI), Leivo Markku (VTT)

To be cited as:

Mladenovic, A., E. Neeft, G. Deissmann, R. Dähn, G. Geng, G. Koskowski, and L. Markku (2019): **ILW: Report describing the selected experiments and the existing/expected experimental results**. Final version as of 24.12.2019 of deliverable D2.11 of the HORIZON 2020 project EURAD. EC Grant agreement no: 847593.

Disclaimer

All information in this document is provided "as is" and no guarantee or warranty is given that the information is fit for any particular purpose. The user, therefore, uses the information at its sole risk and liability. For the avoidance of all doubts, the European Commission has no liability in respect of this document, which is merely representing the authors' view.

Acknowledgement

This document is a deliverable of the European Joint Programme on Radioactive Waste Management (EURAD). EURAD has received funding from the European Union's Horizon 2020 research and innovation programme under grant agreement No 847593.

Status of deliverable		
	By	Date
Delivered (Lead Beneficiary)	A. Mladenovic (ZAG)	2019-12-09
Verified (WP Leader)	D. Jacques (SCK CEN)	2019-12-18
Reviewed (Reviewers)	SCK CEN	2020-01-10
Approved (PMO)	Laurent TRENTY on behalf of the PMO	2020-08-27
Submitted to EC (Coordinator)	Andra	2020-09-28

Executive Summary

The main objective of the EURAD project ACED (Assessment of Chemical Evolution of ILW and HLW Disposal Cells) is to improve methodologies to obtain multi-scale quantitative models for the description of the chemical evolution at the disposal cell scale and to derive robust mathematical models including the most relevant processes.

On interface and waste package scale existing data on materials and material interfaces, are combined with data from currently running experiments and few complementary new experimental set-ups for evaluating the process integration methodology. While on interface scale investigations concentrate on steel-cementitious and steel-clay interfaces, on waste package scale long-term concrete degradation and implications of waste degradation are the focuses.

The subtask 3.1 concerns the first upscaling step from the relatively isolated processes at interfaces to repository sub-systems, representative for IL waste packages, where chemical and physical processes might be closely intertwined.

In case of ILW waste and according to existing ILW concepts in Europe, the subtask 3.1 concentrates on the study of aggregate-cement reactions on 70—100 year old concretes, the degradation of concretes in contact with lay pore water and the analysis of long-term experiments on chemical processes, corrosion and gas generation in waste containers.

These systems allow to studying different aspects of long-term degradation of concrete and waste-concrete interaction.

This deliverable gives a first overview of information already available about existing or currently running experiments:

- A review of information on long term silica aggregate – cement paste interaction (Chapter 2)
- Sampling and initial and planned analysis of 70-100 year old concretes (Chapter 3)
- Leaching experiments of concretes in contact with clay pore water (Chapter 4)
- Long-term experiments on stability of cemented wastes (Chapter 5)

The different modelling approach will begin with the experimental data already available at the beginning of ACED and presented in this deliverable. The modelling work of the long term evolution of ILW waste packages will be done in subtask 3.3.

Table of content

Executive Summary.....	4
Table of content.....	5
List of figures	7
List of Tables	9
Abbreviations.....	10
1 Introduction.....	11
2 A brief review of silica aggregate – cement paste reactions.....	14
2.1 Interfacial reaction between the aggregate and cement paste.....	14
2.2 Factors that accelerate the reaction.....	15
2.3 Alkali-silica-reaction in the presence of Na/K.....	15
2.4 Implications.....	16
3 Field investigation of concrete from the old hydroelectric power plant dams.....	17
3.1 Assessment of the structures.....	19
3.1.1 The Fala hydroelectric power plant.....	19
3.1.2 The Ožbalt hydroelectric power plant.....	20
3.1.3 The Mariborski otok hydroelectric power plant.....	20
3.2 Sampling.....	21
3.2.1 Sampling of concrete at the Fala hydroelectric power plant.....	21
3.2.2 Sampling of concrete at the Ozbalt hydroelectric power plant.....	23
3.2.3 Sampling of concrete at the Mariborski otok hydroelectric power plant.....	24
3.3 Laboratory investigation.....	25
3.3.1 Visual inspection.....	25
3.3.2 Microscopic examination.....	26
3.3.3 Further investigation of the samples from the hydroelectric power plants.....	31
3.4 Outcome and opportunities for modelling.....	33
4 Selected experiments with concrete in contact with clay pore water.....	34
4.1 Concrete recipes.....	34
4.2 Porosity and equilibrium water content.....	35
4.3 Exposure to clay pore water.....	39
4.4 Solid characterisation.....	40
4.4.1 ICP-OES and resistivity (COVRA).....	40
4.4.2 Mineralogical characterisation.....	41
4.4.3 Aggregates (FZJ).....	41
4.4.4 Other tests and characterisations.....	41

EURAD Deliverable 2.11 – ILW: Report describing the selected experiments and the existing/expected experimental results

4.5	Interfaces with Task 2 and Task 4.....	41
4.5.1	Task 2	41
4.5.2	Task 4	41
5	Long-term experiments on stability of cemented wastes - Gas Generation Experiment	42
5.1	Test setup	42
5.2	Results	43
5.3	Summary	46
5.4	Planned work in ACED	46
6	Concluding remarks.....	47
7	References	48

List of figures

Figure 1-1: Organization of ACED (from Jacques et al., 2019).....	11
Figure 1-2: Some potentially important processes that influence long-term chemical evolution on waste package scale.....	12
Figure 3-1: Location of the selected hydroelectric power plants on the Drava River.....	17
Figure 3-2: The Fala hydroelectric power plant (source: http://www.dem.si/en-gb/Power-plants-and-generation/Power-plants/Fala-HPP).....	18
Figure 3-3: The Ozbalt hydroelectric power plant (source: http://www.dem.si/en-gb/Power-plants-and-generation/Power-plants/O%C5%BEBalt-HPP)	18
Figure 3-4: The Mariborski otok hydroelectric power plant (source: http://www.dem.si/en-gb/Power-plants-and-generation/Power-plants/Mariborski-otok-HPP).....	19
Figure 3-5: The “oil corridor”.....	21
Figure 3-6: Location of the boreholes F1, F2 and F3 in the “oil corridor”	22
Figure 3-7: The “control corridor”.....	23
Figure 3-8: Location of the borehole F4 in the “control corridor”	23
Figure 3-9: Concrete bridge with the crane rail	23
Figure 3-10: Location of the borehole V1	23
Figure 3-11: Location of the borehole V2	24
Figure 3-12: Location of the boreholes V3 and V4 on the third turbine pier	24
Figure 3-13: Location of the borehole M1	24
Figure 3-14: Location of the borehole M2	24
Figure 3-15: Typical sample from the Fala hydroelectric power plant (a core with entrapped air)	25
Figure 3-16: Typical sample from the Ozbalt hydroelectric power plant	25
Figure 3-17: Typical sample from the Mariborski otok hydroelectric power plant	25
Figure 3-18: Cracks in quartz aggregate.....	26
Figure 3-19: Cracks in quartz aggregate.....	26
Figure 3-20: Cracks in quartzite aggregate	27
Figure 3-21: Cracks in quartzite aggregate	27
Figure 3-22: Crystalline product (marked by arrow) within the cracks in quartzite aggregate	27
Figure 3-23: Crystalline product (marked by arrow) inside quartzite aggregate	27
Figure 3-24: Quartz grain is cracked but has sharp, straight edges.	27
Figure 3-25: Cracks in the cement paste and within the quartz grains	27
Figure 3-26: Cracks in cement paste and within quartz grains	28
Figure 3-27: Cracks in cement paste and along the grain boundary (in the left hand side)	28
Figure 3-28: Poor contact between quartz grain and matrix	28
Figure 3-29: Porosity at the interface between quartz grain and matrix.....	28

Figure 3-30: Ettringite filling peripheral crack of siliceous aggregate.....	28
Figure 3-31: Occurrence of ettringite in cement matrix	28
Figure 3-32: Ettringite precipitation in air void	29
Figure 3-33: Dedolomitization of dolomite grain.....	29
Figure 3-34: Micro cracks in quartz grain	29
Figure 3-35: Dissolution of cement between quartz grains in sandstone	29
Figure 3-36: Cracks in cement paste and along grain boundary	30
Figure 3-37: Cracks in cement paste and crystalline reaction product in the matrix (marked by arrow)	30
Figure 3-38: Exudation of Ca-rich gel on the surface of the concrete (sample V2)	30
Figure 3-39: Corresponding chemical spectrum of the gel	30
Figure 3-40: Micro cracks in quartz grain (sample M1).....	31
Figure 3-41: Crack along quartz boundary (large grain) and dissolution rim of quartz (small grain) (sample M2).....	31
<i>Figure 3-42: Micro cracks in quartz grain (sample M2).....</i>	<i>31</i>
Figure 3-43: Ettringite in air void (sample M2)	31
Figure 4-1: Equilibrium concentration as a function of relative humidity for backfill concrete with non-oxidised fronts in dark blue.....	36
Figure 4-2: Equilibrium concentration as a function of relative humidity for backfill concrete with uncarbonated areas in purple.....	37
Figure 4-3: Equilibrium concentration as a function of relative humidity of buffer concrete.....	38
Figure 4-4: Exposure to synthetic clay pore water at several stages.....	39
Figure 4-5: Backfill concrete samples exposed to clay pore water.	40
<i>Figure 5-1: Schematic of the GGE showing different types of sampling lines (a, b, c) and online analyses (d) and location of Lines 104, 110, 116, 121, 122 and 123 that were used to take water samples. The dead volumes of the tubing are approximately 0.1–0.4 dm³. Also capsules containing a piece of drum steel and LLW were loaded to the experiment (b, drum solid). Drums are normal size 200 l steel drums (height about 0,9 m and diameter about 0,6 m). (after Small et al., 2008).</i>	<i>43</i>
Figure 5-2: Measured pH of water samples from sample lines from the GGE and fitted average modelled pH of model cells representing tank water and waste drum regions of the experiment.....	44
Figure 5-3: Na, K and Cl, concentration in samples of tank water.	44
Figure 5-4: Measured concentrations of dissolved species in tank water at the drum lid level of the GGE and average modelled concentrations of tank water (a) sulphate and sulphide (b) inorganic and organic carbon (c) iron (d) calcium and magnesium. (Small et.al 2017).....	45

List of Tables

Table 3-1: The selected data on sampling	21
Table 4-1: Concrete recipes buffer concrete and wet density.....	34
Table 4-2: Concrete recipe for backfill concrete; wet density.....	35
Table 4-3: Used recipe for synthetic Dutch poorly indurated clay pore water.....	39

Abbreviations

AAR:	Alkali-aggregate reaction
ACED:	A ssessment of C hemical E volution of ILW and HLW D isposal Cells
ASR:	Alkali-silica reaction
EDS:	Energy-dispersive X-ray spectroscopy
FIB:	Focused ion beam
GGE:	Gas Generation Experiment in Olkiluoto, Finland
HLW:	High-level radioactive waste
ICP-OES:	Inductively coupled plasma mass spectrometry
ILW:	Intermediate-level radioactive waste
ITZ:	Interfacial transition zone
LLW:	Low-level radioactive waste
OPC:	Ordinary Portland cement
SEM:	Scanning electron microscopy
VLJ:	Finnish repository for short-lived low- and intermediate level waste
XAS:	X-ray absorption spectroscopy
XRD:	X-ray diffraction

1 Introduction

The main objective of the EURAD project ACED (Assessment of Chemical Evolution of ILW and HLW Disposal Cells) is to improve methodologies to obtain multi-scale quantitative models for the description of the chemical evolution at the disposal cell scale and to derive robust mathematical models including the most relevant processes.

The ACED approach is focusing on (i) process integration and (ii) model abstraction on three scales, interface scale, waste package scale and disposal cell scale (Figure 1-1).

- In process integration we aim at the integration of existing scientific knowledge (and models) into models at the relevant space and time scales.
- With model abstraction we aim at the development of methodologies to reduce model complexity in a systematic way such that an acceptable description of the chemical evolution is preserved,

For the interface and waste package scale, existing data on materials and material interfaces are combined with data from currently running experiments and few complementary new experimental set-ups for evaluating the process integration methodology. While on interface scale investigations concentrate on steel-cementitious and steel-clay interfaces, on waste package scale long-term concrete degradation and implications of waste degradation are the focus.

The upscaling between the investigated scales is defined in terms of information exchange from relatively small-scale processes (interface scale) to more complex systems at waste package scale and further to full disposal cell scale. The exchange information can take different forms such as identified critical processes, abstracted process representation, up-scaled parameter values, or simplified representation of features.

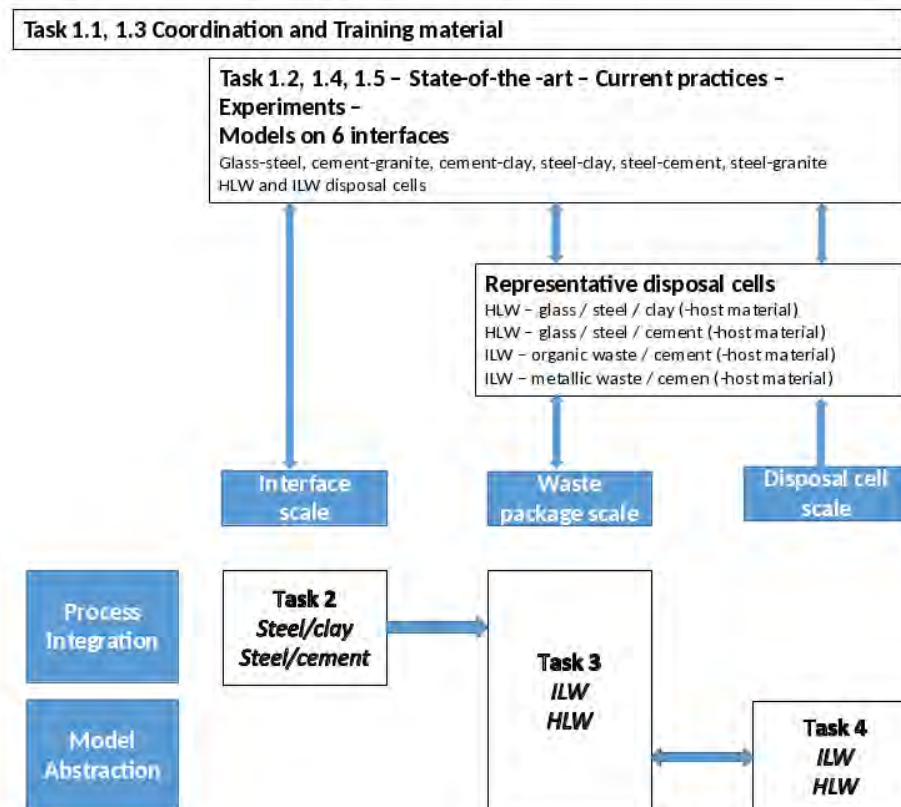


Figure 1-1: Organization of ACED (from Jacques et al., 2019).

EURAD Deliverable 2.11 – ILW: Report describing the selected experiments and the existing/expected experimental results

The work on waste package scale will concentrate on the evaluation of process knowledge integration and model abstraction techniques. For the ILW waste, the focus is on cemented waste packages with metallic (iron/steel) waste and organic waste. Cement is used for waste conditioning and backfilling void space as it provides a stable encapsulant for storage and transport. In addition, the highly alkaline conditions provide a favourable environment for retarding most radionuclides, minimize other chemical reactions like corrosion of iron/steel, and reduce microbiological activity. The long-term chemical evolution of such waste packages in deep geological repositories depends to a large degree on waste package design, waste content and conditioning, and on boundary conditions imposed by the repository design and evolution.

Several processes that are potentially able to lower pH (Figure 1-2) might affect the functionality of the cement barrier:

- The interaction with outer environment might degrade cement materials and lower pH by leaching $\text{Ca}(\text{OH})_2$ from cement phases.
- Aggregate minerals and cement phases might react, in case aggregates are used that are not in thermodynamic equilibrium with cement phases. Specifically siliceous material that cause pozzolanic reaction might lower pH significantly.
- Steel might corrode, consume water and (under reducing conditions) produce H_2 .
- Microbially mediated degradation of organic matter might cause formation of CH_4 and CO_2
- Ingress of CO_2 from outside the waste package or from internal degradation of organic matter might cause carbonation that lowers pH.

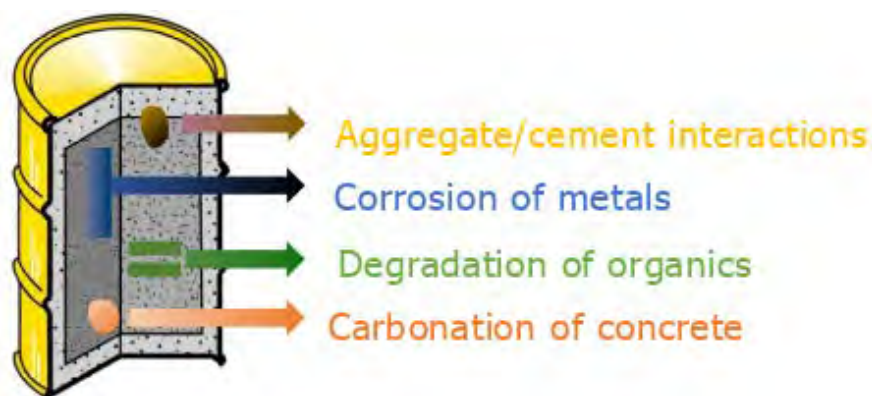


Figure 1-2: Some potentially important processes that influence long-term chemical evolution on waste package scale.

This report reports information on existing data and running experiments that can be used within the project and specific new experiments that will be conducted in Task 3.1.

- For the specific case of very long-term siliceous aggregate-cement paste reactions, we include a short review by PSI of alkali-silica reactions (ASR) and pozzolanic reactions in Chapter 2.
- Aggregate reactivity will be investigated based on samples of 70 to 100 years old concretes from water-saturated parts of hydroelectric power plants that are collected by ZAG (Chapter 3).
- For interaction with the outer environment (concrete in contact with clay pore water) we will use experimental data provided by COVRA (Chapter 4).
- Gas generation (and chemical changes) due to degradation wastes, specifically of organic matter and steel corrosion will be available from running long-term experiments provided by VTT (Chapter 5).

EURAD Deliverable 2.11 – ILW: Report describing the selected experiments and the existing/expected experimental results

- Data on cement/steel interaction will be provided by task 2 and is therefore not specifically investigated in task 3.

2 A brief review of silica aggregate – cement paste reactions

Guoqing Geng, Rainer Dähn, Georg Kosakowski (PSI)

The main hydration products of modern ordinary Portland cement (OPC) is a continuous matrix of calcium silicate hydrates (C-S-H), which hosts crystalline grains such as calcium hydroxide and calcium sulfoaluminate hydrates (Mehta & Monteiro, 2014). These solid phases are in equilibrium with concrete pore solution rich in Ca^{2+} and OH^- . The pore solution may contain Na^+/K^+ depending on the alkaline content in the cement, resulting in a pH in the range of 12.5-13.5 (Lothenbach et al., 2007). During the service life of OPC concrete, reactions may take place between the pore solution and the solid matrix, e.g. the hydration products and the aggregates. Understanding the mechanism of these reactions is key to predict and elongate the durability of concrete (Mehta, 2001). This review focuses on the reaction between cement paste and the siliceous components in aggregate, since this is by far an insufficiently studied issue in the mix-design of concrete used as barriers or containers for long-term geological disposal of radioactive waste (Atkinson et al., 1985).

For the case of siliceous aggregates often two kind of reactions may co-exist, the so-called Alkali-Silica Reaction (ARS) and the pozzolanic reaction. While in the pozzolanic reaction calcium hydroxide reacts with silicic acid and forms C-S-H, for ASR alkali hydroxides (NaOH/KOH) at high pH form an ASR product that is composed of silica and alkali hydroxide plus some calcium. The ASR is often accompanied by a degradation of the matrix and thus a failure of the infrastructure, while the pozzolanic reaction is often promoted as it enhances the strength of concrete.

2.1 Interfacial reaction between the aggregate and cement paste

Aggregates (e.g. gravels and sands) occupy over 60 % volume in an ordinary concrete. In the early application and research of concrete technology, aggregate has been treated as an inert filler of concrete. The early studies postulated a merely physical interaction between aggregate and cement paste, resulting in a porous interfacial transition zone (ITZ) (Scrivener et al., 2004; Ollivier et al., 1995). This porous ITZ forms due to the local accumulation of water on aggregate surface during the early age, which later on hosts the precipitation of large $\text{Ca}(\text{OH})_2$ platelets (Scrivener et al., 2004).

Alkali-aggregate reaction was first identified as a cause of concrete deterioration 80 years ago by T. E. Stanton. After that also other researchers realized that aggregates with different geochemical components may result in different characters of ITZ, implying the presence of chemical interaction between aggregate surface and cement paste at fresh state (Yuan & Odler, 1987; Mehta & Monteiro, 1986; Harutyunyan et al., 2003). For example, limestone aggregate is known to host the preferred orientation of $\text{Ca}(\text{OH})_2$ on its surface, resulting in a porous ITZ and a weak strength (Lothenbach et al., 2008; Tasong et al., 1998; Tasong et al., 1999). Quartz, on the other hand, inhibits the preferred orientation of $\text{Ca}(\text{OH})_2$, thus forming a denser ITZ and a higher bonding strength with the paste (Tasong et al., 1998). The underlying reaction is believed to be the dissolution of quartz which produces Si^{4+} that develops pozzolanic reaction with $\text{Ca}(\text{OH})_2$ (Alexander et al., 1968).

Despite the fact that aggregate may react with the cement paste, the extent of this reaction is usually very limited throughout the service life of modern concrete. This is dominated by the low dissolution rate of silica. For example, at pH~12 the dissolution rate of quartz is in the scale of 10^{-10} and 10^{-9} mol/($\text{m}^2 \cdot \text{s}$), when temperature ranges from 25°C to 60°C (Brady & Walther, 1990; Bickmore et al., 2006; Dove & Elston, 1992). The designed service life of concrete barrier for radioactive waste deposal is up to 100000 years and exceeds the life span of normal concrete infrastructures by far. Therefore, the extent of silica dissolution is far beyond our experience with normal concrete. It is expected that silica will continue to dissolve as long as the pH of the concrete pore solution is buffered at ~12.5 by $\text{Ca}(\text{OH})_2$ (Glasser, 2001). Studies of historical concrete infrastructure have revealed that the outstanding longevity of these material is a result of the pozzolanic reaction between the lime and the (alumino)siliceous constituent (Malinowski, 1979; Moropoulou et al., 2005; Silva et al., 2005). Abundant calcium silicate hydrates were found both in crystalline and amorphous forms (Jackson et al., 2017). On the one hand, this silica-lime

reaction is clearly benefit to the structural integrity of the aged concrete, but on the other hand it will cause a long term reduction in pH which might promote metal corrosion and degradation of organic matter.

2.2 Factors that accelerate the reaction

Although the siliceous aggregates usually exhibit limited reaction in modern concrete, some factors are proven significant to the rate of the aggregate-cement interfacial reaction, for example, the crystallinity of the siliceous components in the aggregate. In case of aggregate containing amorphous or nano-crystalline silica, its fast dissolution may significantly change the ion concentration of the pore solution (Diamond et al., 1981; Diamond, 1997). Researchers reported a clear increase of initial Si concentration in concrete pore solution when reactive aggregate is used. Over the first few hours to the first few days, the Si concentration gradually decreases, along with the decreasing of alkali (Na+K) concentration (Diamond, 1997). It was also reported that the amount and the degree of orientation of $\text{Ca}(\text{OH})_2$ in ITZ is largely affected by the content and reactivity of siliceous component in the aggregate (Okada et al., 2004).

In contrast to the silica in the aggregate, the nano-size silica demonstrates outstanding reactivity and is widely used to produce high performance concrete in recent years (De Larrard & Sedran, 1994; Mazloom et al., 2004; Poon et al., 2006). When silica fume (amorphous SiO_2 sphere, diameter ~10-100 nm) is used as an admixture in concrete, the $\text{Ca}(\text{OH})_2$ content in the hydration product significantly decreases over the first month of hydration (Cheng & Feldman, 1985). This indicates a pozzolanic reaction between the added silica fume and the $\text{Ca}(\text{OH})_2$ precipitates in the relatively early age of concrete. As a result, the porous ITZ filled with large $\text{Ca}(\text{OH})_2$ crystals is modified to a denser matrix filled with calcium-silicate-hydrates, i.e. the product of the pozzolanic reaction. Thus, the strength of concrete is significantly increased. This phenomena is in line with the reduction of concrete porosity when silica fume is added in the mixture (Cheng & Feldman, 1985; Bentz & Stutzman, 1994).

Thermal activation also enhances the reaction of silica-containing aggregates, as widely observed in the steam-autoclaved curing of concrete (Mitsuda et al., 1992; Isu et al., 1995; Yazici et al., 2013). Under a 180 °C autoclaved curing condition, the amount of dissolved quartz ranges between 15% and 45% after 1 hour of curing, depending on the size of the quartz grains (Mitsuda et al., 1992; Isu et al., 1995). The dissolved silica precipitates as tobermorite crystals, forming a densely interlocked matrix with superior mechanical property (Yazici et al., 2013). The elevated temperature clearly enhances the reaction of quartz that is far beyond the reactivity of quartz aggregate in a normal concrete cured at ambient temperature. This implies that the quartz aggregate used in the mix design of geological disposal concrete barrier may develop an over-expectation reaction, since its service condition is likely to be an elevated temperature and pressure environment (Poyet, 2009).

2.3 Alkali-silica-reaction in the presence of Na/K

The early age reaction between siliceous aggregate and cement paste are often beneficial to the densification of cementitious matrix. However, the late age reaction of silica in aggregate often results in a degradation. This reaction takes place between silica and the Na/K content in concrete pore solution, thus denoted as 'alkali-silica-reaction (ASR)' (Ichikawa, 2009; Rajabipour *et al.*, 2015; Haha *et al.*, 2007). The resulted ASR product mainly consisting of silica and alkali hydroxide plus some calcium. In the presence of moisture, this product expands and exerts internal pressure, which generates cracks first in aggregates and later on into hardened cement pastes. ASR damages are among the most commonly diagnosed durability problems for aged infrastructures (Fernandes *et al.*, 2004).

Unlike the general surface reaction of silica at early age, the ASR often takes places at existing micro-cracks in aggregates (Leemann, 2017). Despite years of study, the mechanism of ASR is still not completely understood. Nonetheless, a few parameters are proven largely influencing the dissolution of silica. First, a high pH value of concrete pore solution is necessary to efficiently dissolve silica. This is usually the case for OPC concrete, but not for concrete with pozzolanic admixture such as fly ash and

silica fume (Lothenbach *et al.*, 2011). Second, the presence of alkalis, such as Na and K, largely accelerates the dissolution of silica by forming $\text{SiO-Na}^+/\text{K}^+$ complexations on silica surface (Dove & Elston, 1992). On the contrary, the presence of Al in pore solution seems to inhibit the dissolution of silica (Chappex & Scrivener, 2012; Bernard & Leemann, 2015). The dissolution of silica is under coupled action of all these parameters.

The geochemical nature of the aggregate also dominates its potential of undergoing ASR. Standard tests have been established to evaluate such a potential (Swamy, 2002). For example, aggregate (RILEM TC 191-ARP, 2003) or mortar (RILEM TC 106-AAR, 2000) prisms are immersed in alkaline solutions for a certain period to measure the amount of dissolution or the elongation, respectively. According to the standard tests, two groups of siliceous minerals demonstrate the ability to react and expand when in contact the alkalis in concrete: 1) metastable types of silica (opal, chalcedony, tridymite, cristobalite) including some disordered forms of quartz, 2) alumina–silicate glasses mainly in the matrix of intermediate to acid volcanic rocks (Lindgård *et al.*, 2012; Poole & Sims, 2015). Their reactivity usually increases when the degree of structural order is low and/or the crystallite size is small. Meanwhile, standard tests may fail to predict the reactivity of certain aggregates over long-term exposure to real condition. Aggregates that pass the standard test may exhibit ASR after a few years of service (Lindgård *et al.*, 2012).

Thermodynamic modelling of ASR was not possible due to missing knowledge of the ASR product. Recently such modelling is enabled since the relevant database is established for the ASR products (Shi *et al.*, 2019). ASR products with systematically varying Ca-to-Si ratios and (Na+K)-to-Si ratios were prepared in laboratory and their solution chemistry was measured. The lab-synthesized product was proven to be highly comparable to the ASR product from different affected concrete infrastructures. It should be noted that both the synthesized product and the product from affected concrete are considered the ‘second-stage’ ASR product. The ‘first-stage’ ASR product forming in pre-existing cracks is usually much less crystalline than the ‘second-stage’ product, yet its structure and role in generating the expansion stress is poorly understood (Leemann, 2019). More experimental evidences are needed to solve this puzzle.

2.4 Implications

Glasser (2013) states in his review on use of cements in radioactive waste disposal:

Most Portland cement is combined with mineral aggregate into concretes, grouts and mortars. There is potential in the longer term (>100-1 000 years) for siliceous aggregates to react with cement. This factor, the impact of aggregate on long term performance, has probably received insufficient attention in assessing performance lifetimes especially when cement-based products are used in warm, wet conditions.

In the mix design of concrete container/barrier of radioactive waste, siliceous rocks (e.g. quartz sand) are sometimes used as aggregate. However, there is insufficient evidence whether the siliceous aggregate will develop pozzolanic reaction with Ca(OH)_2 , or would it be vulnerable to ASR damage (Atkinson *et al.*, 1985; Jacques *et al.*, 2014; Kořátková *et al.*, 2017). Although quartz sand is generally inert in the application of ordinary civil infrastructure, it is not in thermodynamic equilibrium with cement phases and its long-term fate remains unclear in the application of radioactive waste disposal. For instance, two factors may significantly promote the dissolution rate of quartz. First, the service life of radioactive waste barrier is designed to be beyond ten thousand years, in contrast to the typical designed life of one century in normal application. Second, a deep geological repository for cemented wastes, like in the case of Switzerland, might be placed in geologic formations with formation temperatures of 40 °C or more. For relatively short times, temperatures might be significantly higher up to 80 °C near certain weakly heat emitting waste sorts and due to hydration of large amounts of cementitious backfill. The reactivity of silica is strongly increased by the elevated temperature. Regarding these factors, more experimental evidence is needed to provide sufficient input for designing and modelling the performance of concrete containers and barriers of radioactive waste.

3 Field investigation of concrete from the old hydroelectric power plant dams

Ana Mladenovic, Alojz Bevc, Pavel Zvanut (ZAG), Rainer Dähn (PSI)

In order to get insight into a long-term aggregate reactivity in concrete structures and thus try to overcome the difficulties in simulating the long term alkali-aggregate reaction (AAR) damage in a structure with short term laboratory test and the translation of the test results to the actual structures, 10 boreholes have been drilled out at three hydroelectric power plant dams. Such data is essential to assess scenarios for ILW and HLW that consider internal degradation of concretes/mortars due to ASR. The selected dams are Fala hydroelectric power plant, Ozbalt hydroelectric power plant and Mariborski otok hydroelectric power plant. All structures are located on the Drava River in the north-east of Slovenia (Fig. 3-1). No historical records of the structures are available; however it is very likely that the cement was transported from the Trbovlje cement plant (established in 1873). It is quite sure that plain cement, without any supplementary materials, was used.

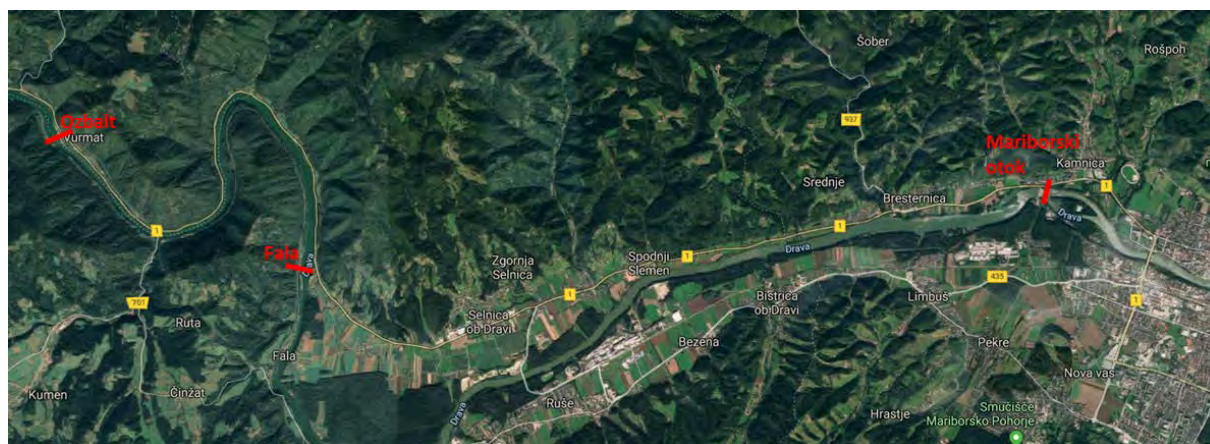


Figure 3-1: Location of the selected hydroelectric power plants on the Drava River

The Fala hydroelectric power plant

The Fala hydroelectric power plant is the fifth power plant in the Slovene section of the Drava River Chain and is the oldest hydroelectric power plant in this section (Fig. 3-2). Its construction began in 1913, with the first five units commissioned in 1918. The sixth unit was built in 1925 and a seventh in 1932. Construction of an eighth unit was completed in 1977. After the extensive refurbishment at the end of the nineteen-nineties, the power plant now operates using only the three newer units. The reservoir has a length of 8.6 km and contains 4.2 million m³ of water, of which 0.9 million m³ can be used for the generation of electric power. The dam was originally built as a structure with five spillways (each with a width of 15 m) allowing for the complete raising of individual groups of spillway gates. Today the old powerhouse has a status of technical heritage and is an interesting point for visitors enabling them to become acquainted with both the old and current methods of operating the power plant.



Figure 3-2: The Fala hydroelectric power plant (source: <http://www.dem.si/en-gb/Power-plants-and-generation/Power-plants/Fala-HPP>)

The Ozbalt hydroelectric power plant

The Ozbalt hydroelectric power plant, with pier-type structure, is the fourth power plant in the Slovene section of the Drava River (Fig. 3-3). It was built between 1957 and 1960 as the twin of the Vuhred hydroelectric power plant which is located upstream. The damming of the Drava River here resulted in a 12.7 km long reservoir containing 10.5 million m³ of water, of which 1.4 million m³ can be used for the generation of power. The dam structure itself is made up of three turbine piers placed between four spillways and the left and right bank buildings. The spilling capacity of all four spillways is 5800 m³/s.



Figure 3-3: The Ozbalt hydroelectric power plant (source: <http://www.dem.si/en-gb/Power-plants-and-generation/Power-plants/O%20balt-HPP>)

The Mariborski otok hydroelectric power plant

This hydroelectric power plant is located near city Maribor, exploiting the energy potential of the Drava River between the Fala hydroelectric power plant and the island on the Drava River (Fig. 3-4). The construction of the power plant had been planned prior to the World War II, but construction only began in 1942. The war caused the construction process to be drawn out considerably so that in May 1945 it was still only 30% completed. In 1948 the commissioning of the first unit was announced, with the

EURAD Deliverable 2.11 – ILW: Report describing the selected experiments and the existing/expected experimental results

second and third units beginning operation in 1953 and 1960. The dam has a 15.5 km long reservoir which contains 13.1 million m³ of water. The dam structure contains three turbine piers placed between four spillways (each 18.75 m wide) and a left and right bank building. These spillways, closed by the double plate hook gates, have a total spilling capacity of up to 5600 m³/s.



Figure 3-4: The Mariborski otok hydroelectric power plant (source: <http://www.dem.si/en-gb/Power-plants-and-generation/Power-plants/Mariborski-otok-HPP>)

The climate conditions

According to the Koeppen-Geiger Classification, the climate in the region can be classified as Cfb climate. It is a typical European continental influenced climate with warm, dry summers and fairly cold winters with snow and frequent fog. In summer, there can be short heat waves, with peaks of 35 °C. The average annual temperature is 9.5°C. The average annual rainfall is 986 mm.

3.1 Assessment of the structures

Regular monitoring has been established on all hydroelectric power plants on the Drava River Chain system. Monitoring has been established in 1970 for the Fala hydroelectric power plant, for the Ozbalt hydroelectric power plant in 1968 and for the Mariborski otok hydroelectric power plant in 1969.

3.1.1 The Fala hydroelectric power plant

The results of performed measurements and visual inspections show that the dam structure is globally stable under static loads. The safety of the dam is within the existing framework.

Deformation measurements

The results of recent measurements of vertical and horizontal displacements, of the inclination of the dam, and of the relative displacements of the expansion joints and cracks, in April 2019, do not show any irregularities in the dam behaviour. Temperature activity of the concrete structure can be seen.

Visual inspection of the dam – concrete surfaces with cracks and other damages

During the last visual inspection of the state of concrete surfaces, in August 2019, it was found that, regarding the state of the examined structure, it is necessary to approach the rehabilitation of individual sites with delaminated concrete. It is also necessary to adequately repair damages of the new floor on the top, especially in the field of concrete crushing.

EURAD Deliverable 2.11 – ILW: Report describing the selected experiments and the existing/expected experimental results

During the last visual inspection of the cracks and other damages, in July 2019, it was found out that the number of cracks did not increase significantly, nor was there any noticeable increase in width or depth of existing cracks - the exception was the machine hall floor (generators No. 9 and 10) where the large number of cracks was found out (caused by vibrations during the operation of the HPP).

3.1.2 The Ožbalt hydroelectric power plant

The results of performed measurements and visual inspections show that the dam structure is globally stable under static loads. The safety of the dam is within the existing framework.

Deformation measurements

The results of recent measurements of vertical and horizontal displacements, of the inclination of the dam, and of the relative displacements of the expansion joints and cracks, in March 2019, do not show any irregularities in the dam behaviour. Temperature activity of the concrete structure can be seen. The exception are the results of measurements of relative displacements of the expansion joints between the riparian structures and the downstream wing walls, which show the excessive settlements of the right wing wall and the excessive horizontal displacement of the left wing wall.

Visual inspection of the dam – concrete surfaces with cracks and other damages

During the last visual inspection of the state of concrete surfaces, in September 2014, we did not observe any specific damage, which would indicate a significant decrease in the durability or safety of the concrete structure.

During the last visual inspection of the cracks and other damages, in December 2018, it was found out that the number of cracks did not increase significantly, nor was there any noticeable increase in width or depth of existing cracks - the exception was the connection corridor in front of the machine hall (especially in front of the generator No. 2).

3.1.3 The Mariborski otok hydroelectric power plant

The results of performed measurements and visual inspections show that the dam structure is globally stable under static loads. The safety of the dam is within the existing framework. The malfunction of the steering system of the upper spillway gate management in December 2017, which caused damage to the dam and the concrete beam of the fourth spillway, did not affect the safety of the dam structure.

Deformation measurements

The results of recent measurements of vertical and horizontal displacements, of the inclination of the dam, and of the relative displacements of the expansion joints and cracks, in April 2019, do not show any irregularities in the dam behaviour. Temperature activity of the concrete structure can be seen.

Visual inspection of the dam – concrete surfaces with cracks and other damages

During the last visual inspection of the state of concrete surfaces, in August 2019, it was found that, regarding the state of the examined structure, it is necessary to approach the rehabilitation of damages in the connection corridor, which were caused by uncontrolled lifting of the spillway gate. As part of the regular maintenance work, it has been proposed to remediate the local sites with delaminated concrete.

During the last visual inspection of the cracks and other damages, in December 2018, it was found out that the number of cracks did not increase significantly, nor was there any noticeable increase in width or depth of existing cracks - the exception was the inspection gallery where, due to the delamination of the protective layer of the concrete, the corroded steel reinforcement was visible in several places.

3.2 Sampling

The sampling from the concrete structures have been performed in accordance to the Sampling Plan, which was prepared on a basis of results obtaining during the regular monitoring of the dams on the Drava River. A drilling machine with a diamond crown of diameter 100 mm was used. The length of the samples was up to 25 cm. Cores have been taken in different exposure environments in areas where cracking was suspected caused by ASR e.g. map cracking, longitudinal cracks or surface exudations. Sampling was carried out in September and November 2019 by ZAG, according to Godart et al (2013) and Jensen (1993). Sufficient precautions were taken during core sampling and subsequent sample preparation to ensure that evidences of ASR are retained. The selected data on the sampling is presented in Table 3-1.

Table 3-1: The selected data on sampling

	Age of the concrete	Number of boreholes	Location
Fala hydroelectric power plant	105 years	4	indoor
Ozbalt hydroelectric power plant	62 years	4	outdoor
Mariborski otok hydroelectric power plant	74 years	2	indoor

3.2.1 Sampling of concrete at the Fala hydroelectric power plant

Four boreholes, designated as F1, F2, F3 and F4 have been drilled. Three sampling locations (F1, F2 and F3) were located in the “oil corridor” (Figs. 3-4 and 3-5), where the relative humidity is between 70% and 80%. Sample F4 has been taken from concrete in the “control corridor”, where relative humidity is above 90% (Figs. 3-6 and 3-7). Both corridors are situated in the old part of a dam, built in 1918.



Figure 3-5: The “oil corridor”



Figure 3-6: Location of the boreholes F1, F2 and F3 in the “oil corridor”

Sample F1 has been drilled out at the location of the wide cracks with widths of up to several mm, running in the vertical and horizontal directions. Sample F2 has been drilled out in the area where only a few vertical cracks have been confirmed, however the surface was covered with efflorescence and exudations. Sample F3 has been drilled in the area of intensive map-cracking. Location of sample F4 was at the area of intensive exudation of calcium carbonate; however It was not possible to detect potential cracks due to recent repair works



Figure 3-7: The “control corridor”



Figure 3-8: Location of the borehole F4 in the “control corridor”

3.2.2 Sampling of concrete at the Ozbalt hydroelectric power plant

Four boreholes, designated as V1, V2, V3 and V4 have been drilled. All samples have been drilled out outdoor, V1 and V2, on the bridge with crane rail (Figs. 3-8, 3-9, and 3-10), and V3 and V4 on the third turbine pier (Fig. 3-11).



Figure 3-9: Concrete bridge with the crane rail



Figure 3-10: Location of the borehole V1



Figure 3-11: Location of the borehole V2

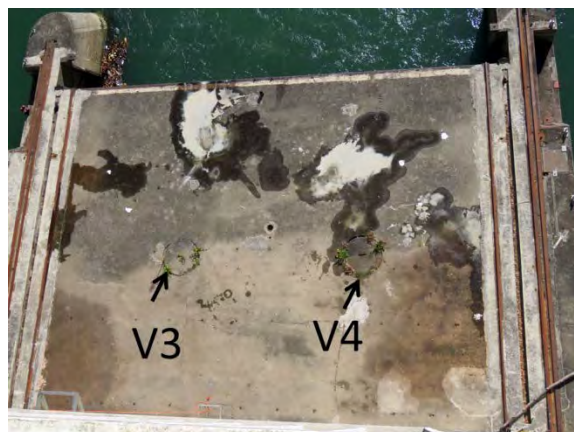


Figure 3-12: Location of the boreholes V3 and V4 on the third turbine pier

Samples V1 and V2 has been drilled out at the location of the random cracks filled with white and yellowish exudations and precipitation. Intensive surface discoloration has been observed. Samples V3 and V4 are in the area where surface rehabilitation has been recently carried out and is therefore with no visual cracks.

3.2.3 Sampling of concrete at the Mariborski otok hydroelectric power plant

Two boreholes, designated as M1 and M2 have been drilled. Both samples were located in the storage room, with an average relative humidity 60 %. All samples have been drilled out outdoor, V1 and V2, on the concrete bridge with the crane rail (Figs. 3-8, 3-9 and 3-10), and V3 and V4 in the third turbine pier (Fig. 3-11).



Figure 3-13: Location of the borehole M1



Figure 3-14: Location of the borehole M2

3.3 Laboratory investigation

3.3.1 Visual inspection

Visual inspection using a low power stereo microscope revealed the same type of aggregates in all samples of concrete; a mixture of siliceous and carbonate sand and gravel, up to 32 mm. The grains are semi-rounded to rounded. The main components are quartz, quartzite, sandstone, siltstone, gneiss and amphibolite, as well as limestone and dolomite. This type of siliceous aggregates is considered as a slow-reacting aggregate. The mass ratio between siliceous and carbonate aggregate is approximately 60:40. The concrete samples from the Fala hydroelectric power plant are nonhomogeneous, porous, with large voids, cavities and parts where the cement matrix has been leached out (Fig. 3-14). The concrete samples from the Ozbalt hydroelectric power plant are much more homogeneous, well compacted, with low porosity and good contact between aggregate and matrix (Fig. 3-15). Similar characteristics have been revealed on the samples from the Mariborski otok hydroelectric power plant (Fig. 3-16). No clear signs of ASR reaction in term of rims, gel exudations or cracks have been observed during the macroscopic examination.



Figure 3-15: Typical sample from the Fala hydroelectric power plant (a core with entrapped air)



Figure 3-16: Typical sample from the Ozbalt hydroelectric power plant



Figure 3-17: Typical sample from the Mariborski otok hydroelectric power plant

3.3.2 Microscopic examination

The morphology and microstructure of the concrete mixtures were analysed on polished specimens in the transverse direction, in the JEOL 5500 LV SEM and JEOL JSM-IT500, which were coupled to an Oxford energy dispersive spectrometer, using backscattered electrons and a low vacuum. Examination of fractured samples has also been performed. The aim of these laboratory tests was to assess the degree of ASR in the concrete samples and the extent of this reaction.

The analysis focused mainly on the samples from the oldest dam (the Fala hydroelectric power plant), although the samples from other two locations were also examined.

3.3.2.1 Concrete samples from the Fala hydroelectric power plant

The analysis of all samples revealed that ASR is present in the investigated concrete cores. The signs of reaction are clear and involve both coarse and fine aggregate particles. Internal cracks, mostly in quartz, quartzite and gneiss are the most distinguish parameter of degradation. ASR occurs in different forms. The most frequent features are micro cracks in quartz grains (Figs. 3-17 – 3-20). Grains of quartzite and gneiss are cracked along its grain boundaries. Cryptocrystalline reaction products in reacted aggregates have been identified in few cases (Figs. 3-21 and 3-22). Typical lime-alkali-silica gels or pure gels have not been observed. Some grains of quartz aggregate are shown in Figure 25, where it can be seen that the grains are cracked but have sharp, straight edges. All samples show a distinct crack pattern including radial cracks running from aggregates into the hardened cement paste (Figs. 3-24 – 3-26). Some cracks also cut the quartz grains or run along boundary between the cement matrix and the grains. The contact between the siliceous grains and the cement paste is poor (Fig. 3-27), and at the interface relatively high porosity occurs as a result of ASR (Fig. 3-28).

In some parts of the concrete samples a large amount of ettringite formed next to the aggregate particles (Fig. 3-29), as well as in the cement matrix (Fig. 3-30) and in air voids (Fig. 3-31). Some dolomite grains exhibit a dedolomitization rim, however it does not seem this reaction is deleterious (Fig. 3-34).

There are no significant differences between examined samples (F1 – F4). ARS is present in all samples, there are slight variation in intensity of reaction within each specimen, which is related to the porosity of the concrete. Parts with higher porosity are more affected.

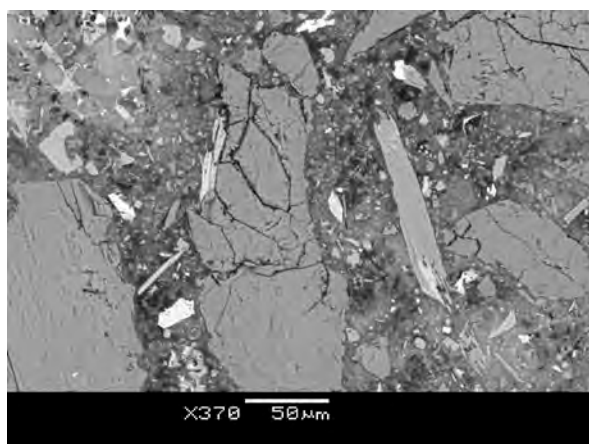


Figure 3-18: Cracks in quartz aggregate

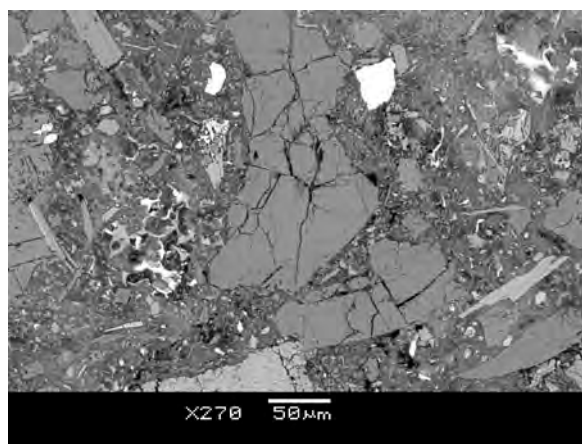


Figure 3-19: Cracks in quartz aggregate

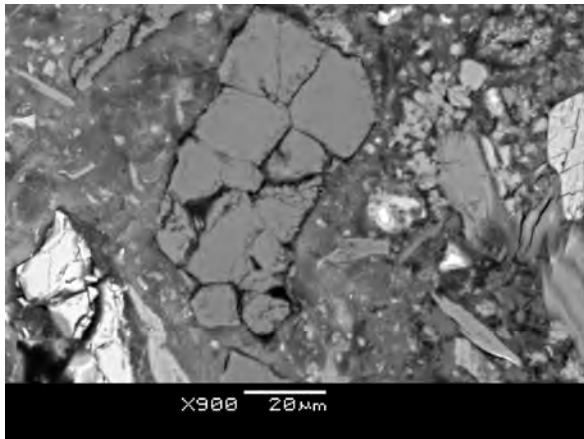


Figure 3-20: Cracks in quartzite aggregate

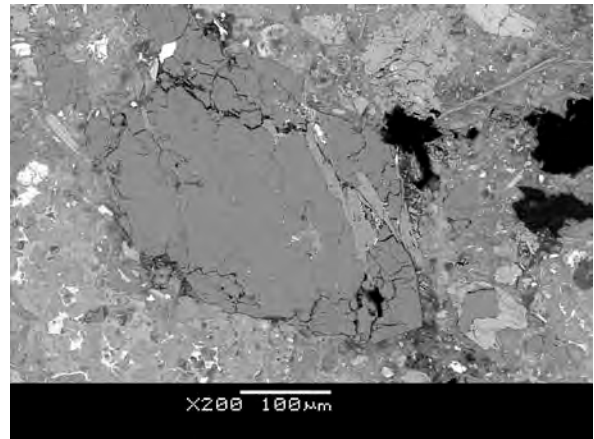


Figure 3-21: Cracks in quartzite aggregate

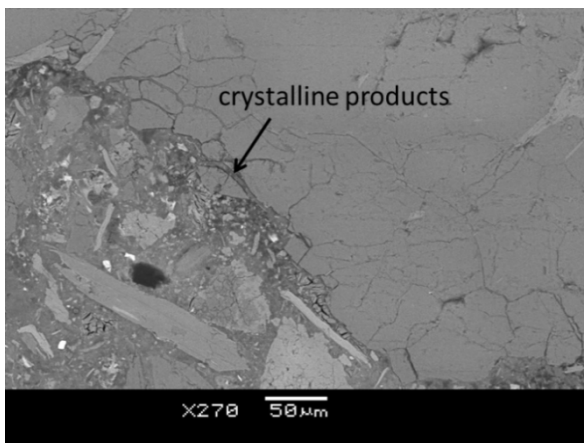


Figure 3-22: Crystalline product (marked by arrow) within the cracks in quartzite aggregate

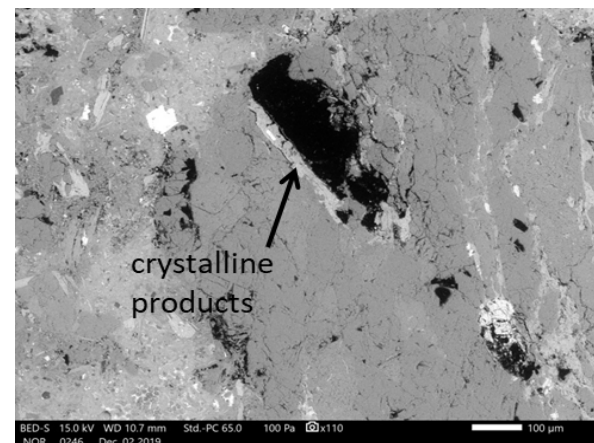


Figure 3-23: Crystalline product (marked by arrow) inside quartzite aggregate

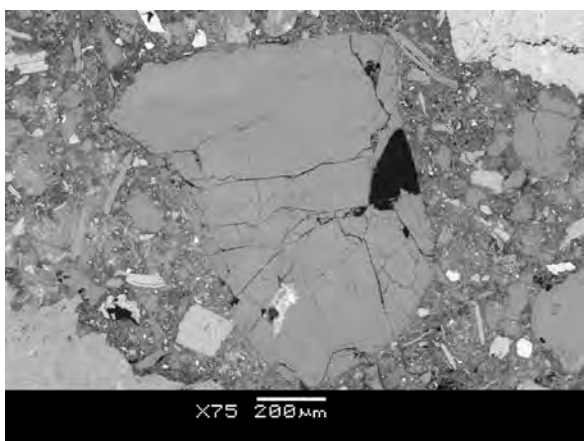


Figure 3-24: Quartz grain is cracked but has sharp, straight edges.

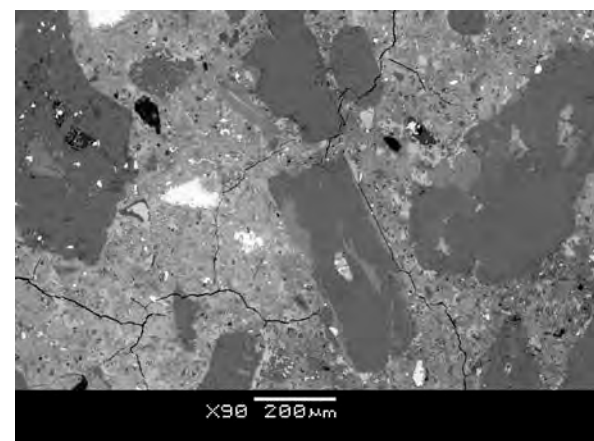


Figure 3-25: Cracks in the cement paste and within the quartz grains

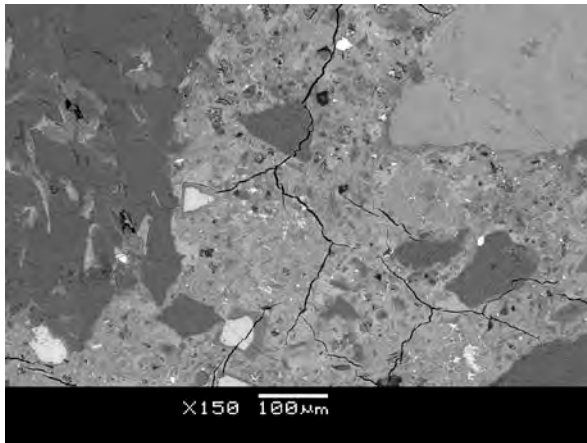


Figure 3-26: Cracks in cement paste and within quartz grains

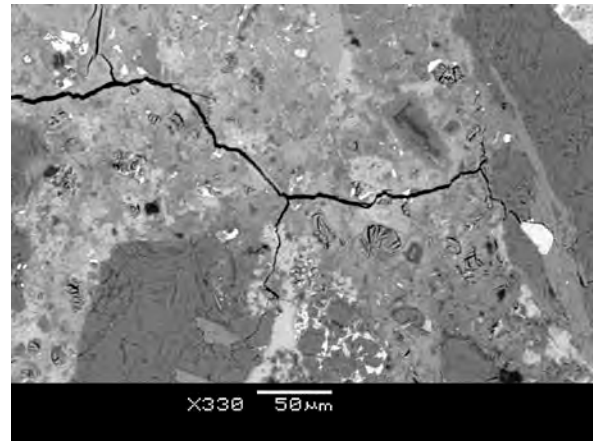


Figure 3-27: Cracks in cement paste and along the grain boundary (in the left hand side)

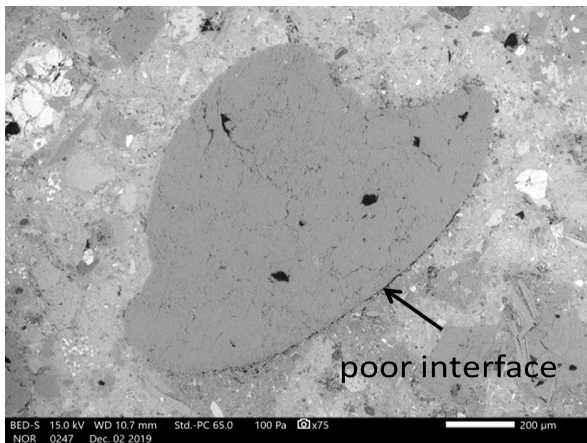


Figure 3-28: Poor contact between quartz grain and matrix

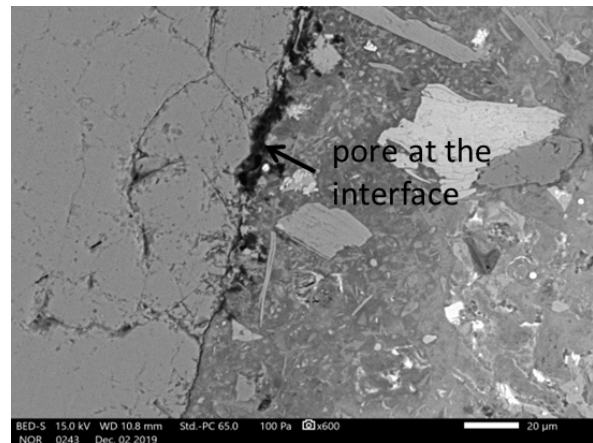


Figure 3-29: Porosity at the interface between quartz grain and matrix

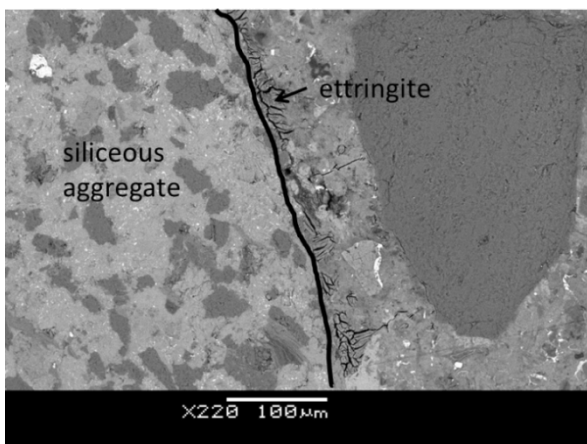


Figure 3-30: Ettringite filling peripheral crack of siliceous aggregate

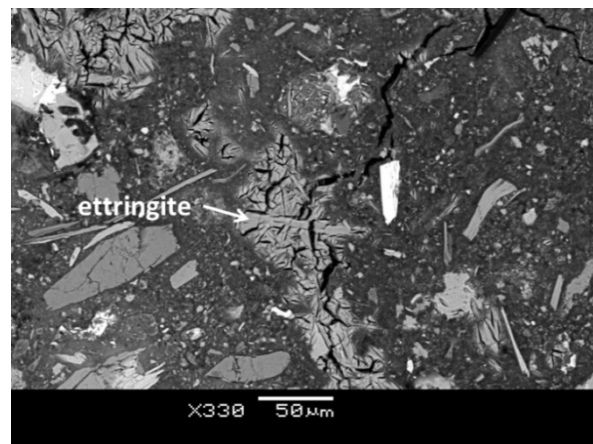


Figure 3-31: Occurrence of ettringite in cement matrix

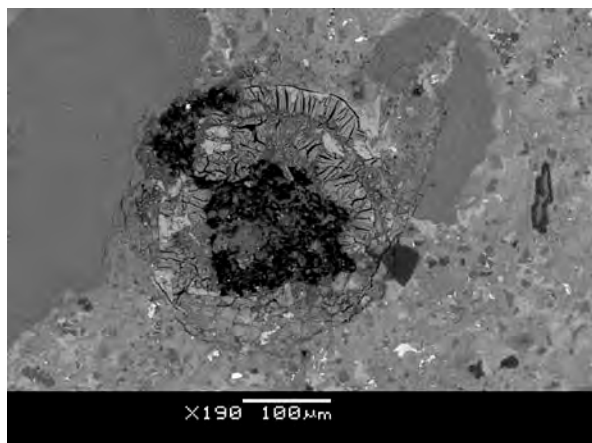


Figure 3-32: Ettringite precipitation in air void

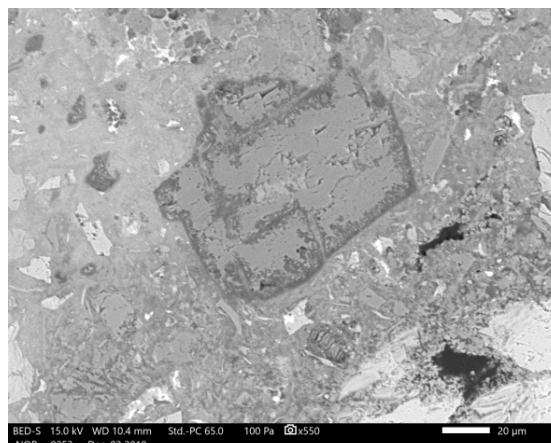


Figure 3-33: Dedolomitization of dolomite grain

3.3.2.2 Concrete samples from the Ozbalt hydroelectric power plant

In all four concrete samples (V1 - V4) signs of ASR have been observed. Grains of siliceous aggregate (both coarse and fine) exhibit ASR which is manifested in the form of micro cracks in quartz grains (Fig. 3-34), and micro cracks in quartzite, gneiss in other siliceous grains containing quartz as one of the main constituents. This indicates that the silica cement binding the subgrains in these petrographic types dissolves more readily than the subgrains themselves (Fig 3-35). In contrast to the samples from the Fala hydroelectric power plant, the dissolution of the siliceous grains appears more advanced. Many micro cracks intersecting cement matrix running from aggregates into hardened cement paste have been observed (Figs. 3-36 and 3-37). The reaction products are either a lime-alkali-silica gel, which was identified on the surface of the samples V1 and V2 (Fig. 3-38) or microcrystalline product which was observed in the cement matrix and with morphology of the gel surrounding a flint particle, with the corresponding chemical spectrum in Figure 3-39. The CaO/SiO₂ ratio of the gel was between 0.3 and 1.6. Large amounts of ettringite were also found filling cracks in the cement paste and along the siliceous grains.

All samples were taken at the exposed locations of the Ozbalt hydroelectric power plant. There are no significant differences between examined samples (V1 – V4). The signs of reaction in their features were compared to the signs observed at the Fala hydroelectric power plant, however they were more intensive and reaction products occurred in larger quantities.

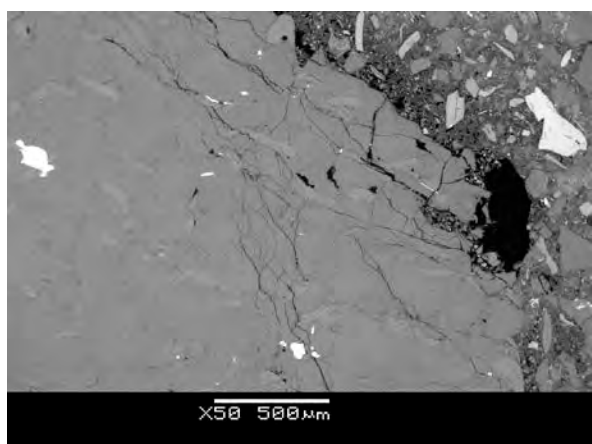


Figure 3-34: Micro cracks in quartz grain

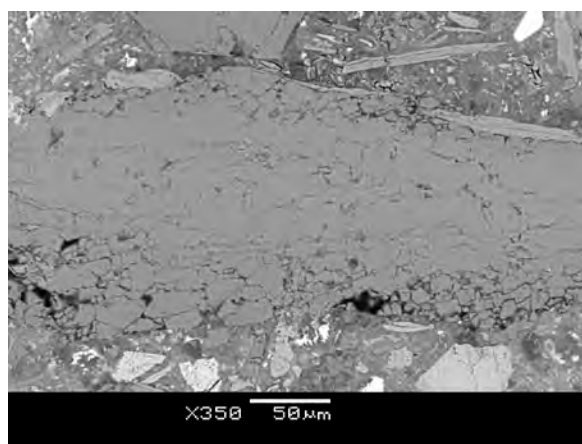


Figure 3-35: Dissolution of cement between quartz grains in sandstone

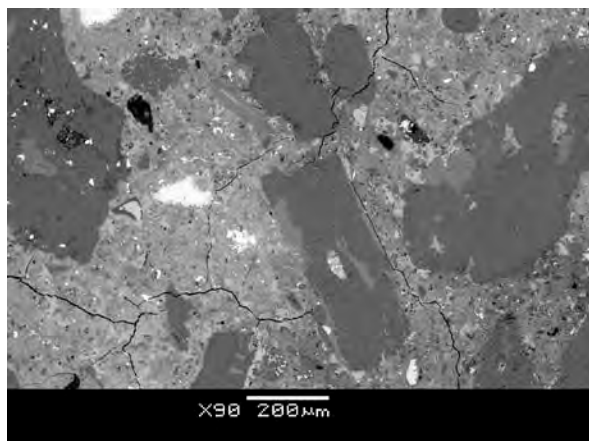


Figure 3-36: Cracks in cement paste and along grain boundary

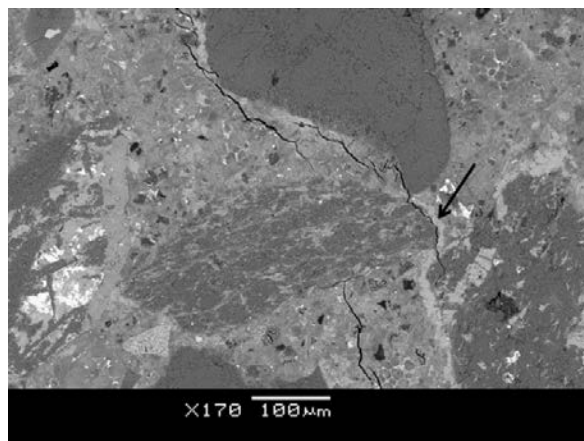


Figure 3-37: Cracks in cement paste and crystalline reaction product in the matrix (marked by arrow)

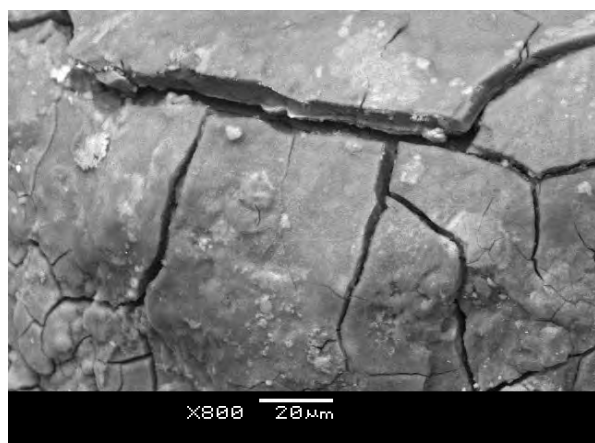


Figure 3-38: Exudation of Ca-rich gel on the surface of the concrete (sample V2)

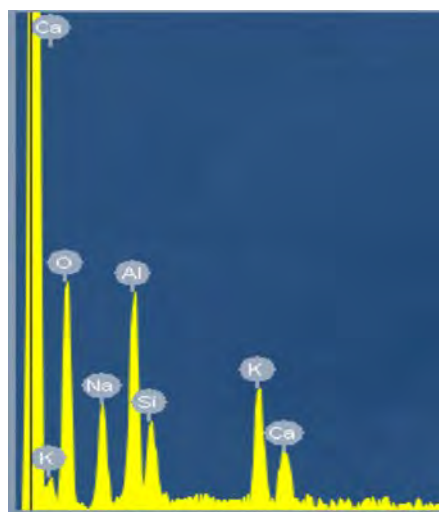


Figure 3-39: Corresponding chemical spectrum of the gel

3.3.2.3 Concrete samples from the Mariborski otok hydroelectric power plant

Concrete samples from the Mariborski otok hydroelectric power plant exhibit only slight signs of reaction or degradation. Individual grains of quartz with cracks and dissolution features were detected (Figs. 3-40, 3-41 and 3-42). The fine aggregates are affected while the coarse grains do not show any indications of degradation. In some pores precipitation of ettringite has been observed (Fig. 3-43).

Dissolutions areas in quartz also occur (Fig 3-41), in the direction from the outside towards the interior of the grain. Neither reaction products nor cracks across the cement paste were observed.

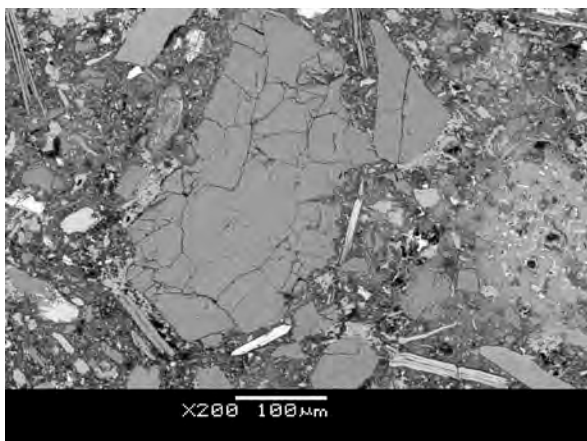


Figure 3-40: Micro cracks in quartz grain (sample M1)

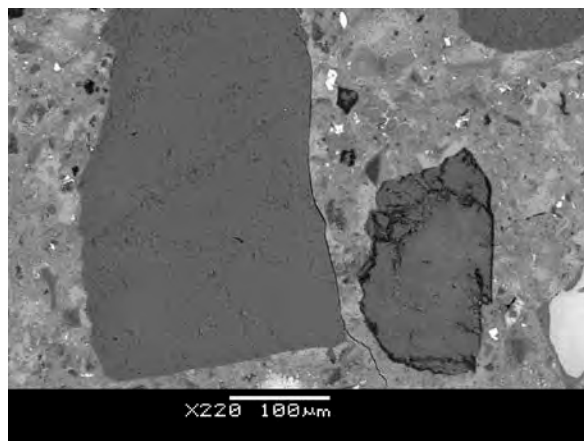


Figure 3-41: Crack along quartz boundary (large grain) and dissolution rim of quartz (small grain) (sample M2)

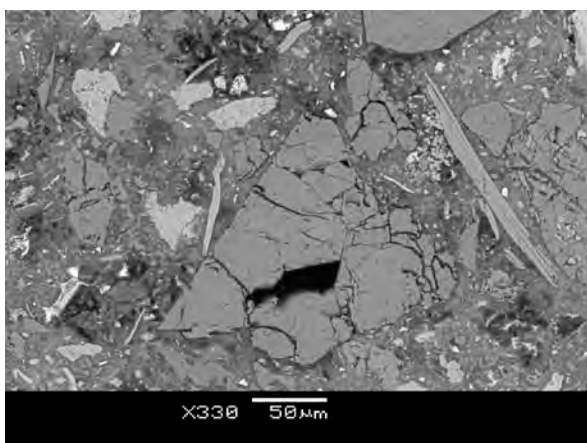


Figure 3-42: Micro cracks in quartz grain (sample M2)

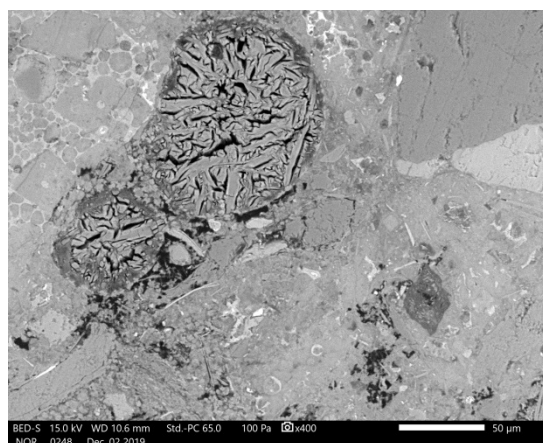


Figure 3-43: Ettringite in air void (sample M2)

3.3.3 Further investigation of the samples from the hydroelectric power plants

The ARS affected concrete samples from the hydroelectric power plants will be further investigated in order to get more accurate input for modelling part in WP3.3. RILEM ARR-4.1, test method (Detection of potential alkali-reactivity – 60°C accelerated method for testing aggregate combinations using concrete prisms) will be deployed in the first phase to detect the potential and extent of the ASR reactions in hydroelectric power plants. This is an accelerated treatment of samples in alkaline solution at relative humidity 100% and temperature 60°C. The duration of the test is 20 weeks. After this treatment is finished the samples will be examined for ASR development, focusing on the potential changes in microstructure in comparison to the current characteristic/pathology features of the samples and on degradation state in terms of chemistry (pH dependence, portlandite depletion, C-S-H characteristics, and fate of other mineral phases in the concrete). Also the development of degradation, type of affected aggregates, degree of crystallinity of quartz, composition and morphology of gel, propagation of cracks, mineralogical changes in cement matrix, other signs of pathology will be

assessed. Optical microscopy and scanning microscopy (SEM/EDS and FESEM/EDS and TEM) will be utilized for performing this second phase of research as well as TGA.

3.3.3.1 Investigation of old concrete samples with micro-XRD (PSI)

Modern synchrotron-based spectroscopic and scattering techniques offer the opportunity to probe interface and surface structures down to the atomic length scale and gain data of exceptional quality for structural studies. For example, the analysis of aggregate-cement reaction products formed under different boundary conditions with state-of-the-art synchrotron-based methods will reveal their structure and improve the understanding on their formation and the mechanisms of formation. Spatially resolved X-ray diffraction (micro-XRD) combined with micro-X-ray fluorescence (micro-XRF) will allow to gain spatially resolved micro-scale information to pin down the influence of the heterogeneity of the complex phase system in concretes. The synergistic use of micro-XRF with micro-XRD opens up the possibility of determining the element distributions in the complex ASR zones and subsequent the structural refinement of crystalline phases.

Application of micro-XRD on concretes

XRD allows to gain atomic level information on the long-range crystallographic order, in contrast to X-ray absorption spectroscopy, which provides atomic level information at the short-range crystallographic order (up to ~ 5 Å around the X-ray absorber). Interpretation of diffraction experiments carried out on cements can be a challenging task since many crystal grains from different structures can contribute to the diffraction pattern. Depending on the ratio between the crystal size and the X-ray beam spot size, the quality of the diffraction data in such samples ranges from almost perfect individual single crystal characteristics to microfine powder or even non-crystalline materials. In the case of micro-diffraction on a polycrystalline sample it is very likely that there are several crystallites in the beam, diffracting into a single image. These crystallites may be small compared to the size of the X-ray beam and thus be randomly oriented, so that only a powder pattern can be registered. Therefore, we developed an approach in which micro-XRD can be applied to cementitious thin sections which were rotated in the X-ray beam (Dähn et al., 2016; Dähn et al., 2014). In this approach the collected XRD frames of the rotated sample are summed up into a composite pattern, which is then integrated from a two dimensional (2D) image into a classical 1D powder pattern. The data analysis is then performed as in a classical powder diffraction experiment, in which the phase identification by a search in database and a Rietveld refinement can be carried out.

Based on the tools developed in the earlier study (Dähn et al., 2014) we applied successfully micro-XRD to characterize the mineral phases formed in micro-cracks of concrete aggregates as a consequence of ASR (Dähn et al., 2016). This high spatial resolution technique enabled, for the first time, to directly gain structural information on ASR products formed in a 40-year old motorway bridge damaged due to ASR. Micro-XRD pattern were collected at selected points of interest along a vein by rotating the sample. Rietveld refinement determined the structure of the ASR product consisting of a new layered framework similar to minerals from the mountainite family. Whereas the study unequivocally demonstrated that the reaction product formed after 40 years of reaction is crystalline, no information is available on the initial reactions occurring over weeks.

Application of micro-XRD in this study

The experiments require the following:

1. Preparation of thin (~ 30 micron thick) sections of the ASR products, in case intact samples are foreseen for investigations. The sample should be free standing or on a support which does not

EURAD Deliverable 2.11 – ILW: Report describing the selected experiments and the existing/expected experimental results

- hamper micro-XRD measurements in transmission mode (for details see (Dähn et al., 2016; Dähn et al., 2014))
2. An SEM/EDS characterisation of the thin sections.
 3. In case 3d-micro-XRD experiments are needed a FIB preparation of cylinders or cubes less than a diameter of 70 µm.

There will be a need for access to synchrotron beamtime to carry out the proposed study. For the measurements we will apply for beam time by submitting proposals. Most synchrotron offer this possibility twice per year. For successful proposals an SEM analysis would be important to be included. Beamlines offering these techniques include the Swiss Light Source (Villigen, Switzerland), Diamond Light Source (Harwell, UK), Advanced Light Source (Berkeley, US), SSRL (Stanford, US), Advanced Photon Source (Lemont, US).

The investigations will require synthetic references which will allow to compare their XRD pattern with the one obtained from in situ ASR samples.

In case time and budget allows X-ray absorption spectroscopic (XAS) investigations could be employed. XAS can be employed to determine the local structure (bond distance, coordination numbers and type of near neighbours) around an X-ray adsorbing atom in a crystalline or amorphous structure. Spectra of elements of interest (Ca, K, Na) can be compared with spectra of adequate reference compounds, i.e. characteristic fingerprints in the spectra can be exploited. XAS deploys its most power if coupled with advanced theoretical calculations, however given the time und budget conditions these seem not be possible in the foreseen project.

3.4 Outcome and opportunities for modelling

Petrographic examination of concrete cores revealed that deleterious ASR is present in all investigated concretes samples from all three hydroelectric power plants. The most severely affected are concrete samples from the Ozbalt hydroelectric power plant. These samples were taken from the structure outdoor in atmospheric conditions. Since no movement of structural elements caused by volume expansion and deformation of concrete have been observed at any of the dams, it can be concluded that at this moment ASR-related damage is low and the magnitude of the reaction is not sufficient to produce significant problems of serviceability or structural function.

However in term of long term stability of quartz and quartz-bearing siliceous aggregate a significant dissolution and tendency to micro-cracking has been observed. Another type of degradation which has also been confirmed in the concrete samples is secondary ettringite formation, which degrades C-S-H and Ca(OH)_2 and thus decreasing pH. Taking into account this coexisting degradation process it might be expected that the rate of silica dissolution will slowly decrease.

The experimental findings on changes in cement mineralogy can be used to calibrate thermodynamic models for concrete degradation upon dissolution of aggregates. Of special interest are quantitative information on the degree of aggregate dissolution, as they are needed to parametrize kinetic models for aggregate mineral dissolution. Such kinetic models are the key to associate a time scale to concrete degradation by aggregate dissolution.

4 Selected experiments with concrete in contact with clay pore water

Erika Neeft (COVRA), Guido Deissmann (FZJ)

COVRA has exposed cubical samples of concrete to synthetic clay pore water at room temperature since September 2016. Poorly indurated clay is the clay host rock investigated in the Netherlands. These clays have a porosity of around 40% (Mazurek, 2008). The conditioning concrete (or buffer concrete) as well as the envisaged backfill concrete have a smaller porosity than this clay host rock i.e. 12-13% for the buffer concrete and 24-25% for the backfill concrete. Representative results for reaction fronts within concrete during geological disposal are expected with this experiment since the diffusion values for dissolved species within the clay host rock are expected to be larger than the diffusion values within both types of concrete. The interpretation of these reactions can be used to predict concrete alteration. It depends on the safety function of the concrete barrier whether this alteration can be characterised as concrete degradation. Minor chemical effects within concrete as a result of the steel-concrete interface in the disposal concept are investigated as well, since dissolved iron is expected to be present in Dutch clay pore water and therefore added to the exposure medium.

4.1 Concrete recipes

The concrete samples have been made by COVRA's concrete expert; the samples have been mechanically approved and the variation in density is less than 2%. The characteristic compressive strength for the buffer concrete needs to be larger than 45 MPa and for backfill concrete more than 10 MPa. The following tables show the concrete recipes to make cubical samples with the following edges 5 cm, 10 cm and 15 cm. The wet density has been determined by NEN-EN 12350-6 for the buffer concrete made in 2015 and the casted weight and dimensions less than 1 day after pouring and vibration for the batch made in 2016 and backfill concrete. Backfill concrete is foamed concrete i.e. a porous grout. The following tables show the concrete recipes in which the underlined densities have been used to determine the concentration of each component with the weighted proportions.

Table 4-1: Concrete recipes buffer concrete and wet density

Component	Type	Batch 2015 N=6		Batch 2016 N=51 (75)
		<u>2315</u> & 2311 kg m ⁻³ <u>2286</u> & 2299 kg m ⁻³	kg m ⁻³ for each component	
Cement	CEM III/B 42.5 LH/SR	385	421	402
Water	-	176	180	184
Plasticiser	TM OFT-II B84/39 CON. 35% (BT-SPL)	5	6	5
Fine aggregate	Quartz sand : 0-4 mm	846	860	827
Coarse aggregate	Quartz gravel : 2-8 mm	865	848	866

Table 4-2: Concrete recipe for backfill concrete; wet density

Component	Type	Batch 2016 $1695 \pm 35 \mu \pm \sigma \text{ kg m}^{-3}$ N=60
		kg m ⁻³ for each component
Cement	CEM III/B 42.5 LH/SR	411
Water	-	144
Plasticiser	TM OFT-II B84/39 CON. 35% (BT-SPL)	4
Foaming agent + water	TM 80/23	5
Fine aggregate	Quartz sand : 0-2 mm	1131

4.2 Porosity and equilibrium water content

Cubical samples could be casted from moulds with an inner edge of 5 cm or sawn from cubical samples with an edge of 150 cm. The resulting cubical samples with an edge of 5 cm have been submerged in tap water for at least 5 months for buffer concrete and at least 4 months for backfill concrete in order to obtain fully water saturated samples. After that, these samples have been exposed to different relative humidity's for at least 997 days at 20°C and 5°C. The weights of the samples have been regular measured and the saturation of the salt solutions to obtain the relative humidity's, have been monitored. Salt has been added in the case that under saturation occurred. The following figures show the equilibrium concentration at 20 degrees Celsius for buffer and backfill concrete; the equilibrium concentration at 5 degrees Celsius is being made. The gravimetrical determined porosity is 12-13% for buffer concrete and 24-25% for backfill concrete. Attempts have been made to measure the resistivity but most of the measurements indicated a resistivity out of the experimental range.

The transient weights will be modelled to determine the parameters for non-linear diffusion of water (two phase flow) in these two types of concrete. The samples have been mechanically tested and split surfaces of concrete have been made to observe the intrusion of oxygen. The oxygen fronts are grey i.e. containing traces of FeSO₄ and non-oxidized areas of concrete are blue i.e. containing traces of FeS₂. The images will be interpreted with numerical modelling. A phenolphthalein solution was sprayed on the surfaces according to NEN-EN 14630 in order to observe the carbonation front. Photos of these reaction fronts have been added to the equilibrium concentration of backfill concrete and will also be available for the buffer concrete. These reaction fronts will also be interpreted with numerical modelling. All cracked samples have been preserved in order to be used for further analysis e.g. the drying may help to characterise the CSH phases. There is also a cubical concrete sample available that has been fabricated in 1993 with CEM III/A instead of CEM III/B which may to identify when ASR may occur.

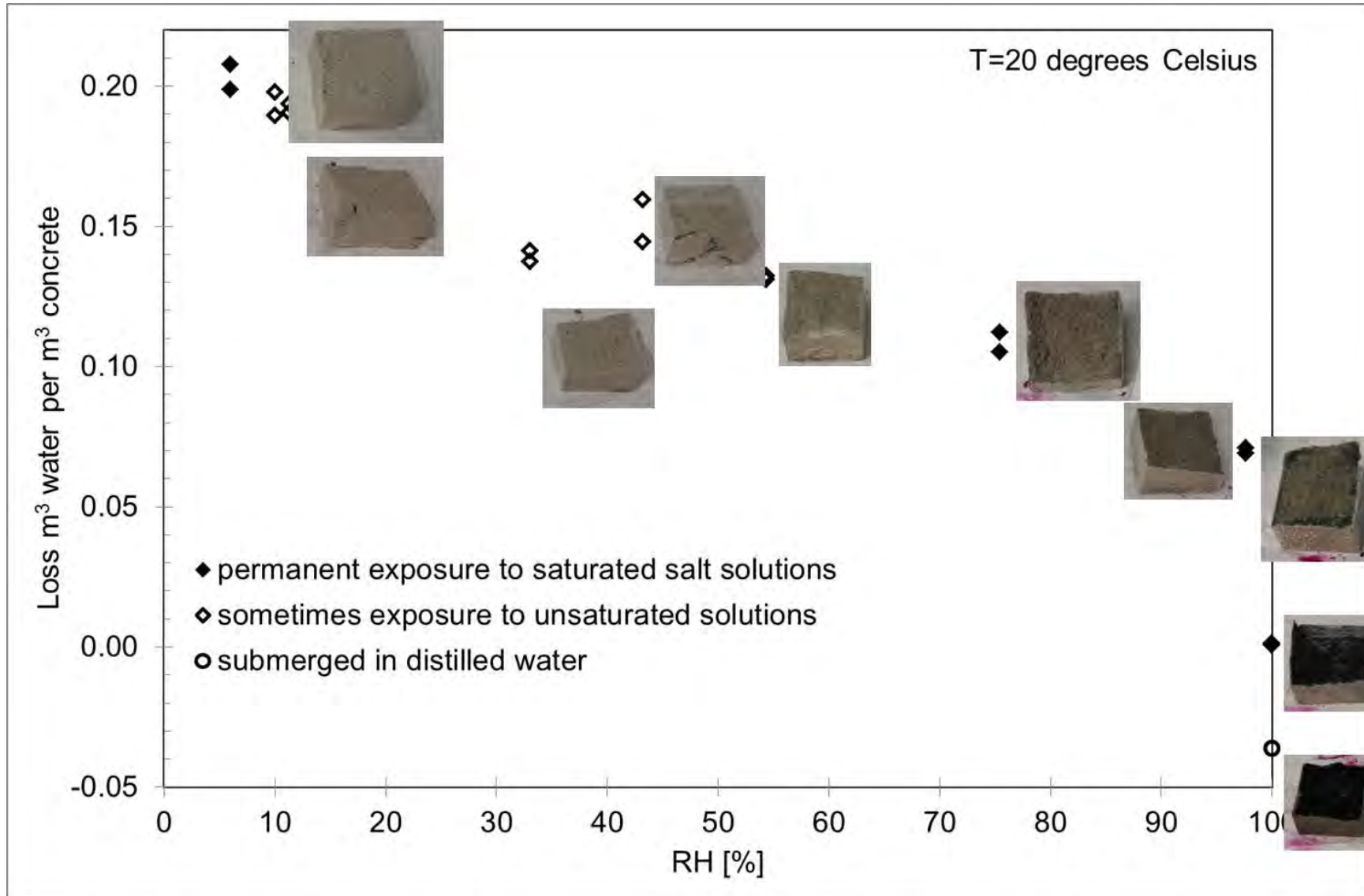


Figure 4-1: Equilibrium concentration as a function of relative humidity for backfill concrete with non-oxidised fronts in dark blue.

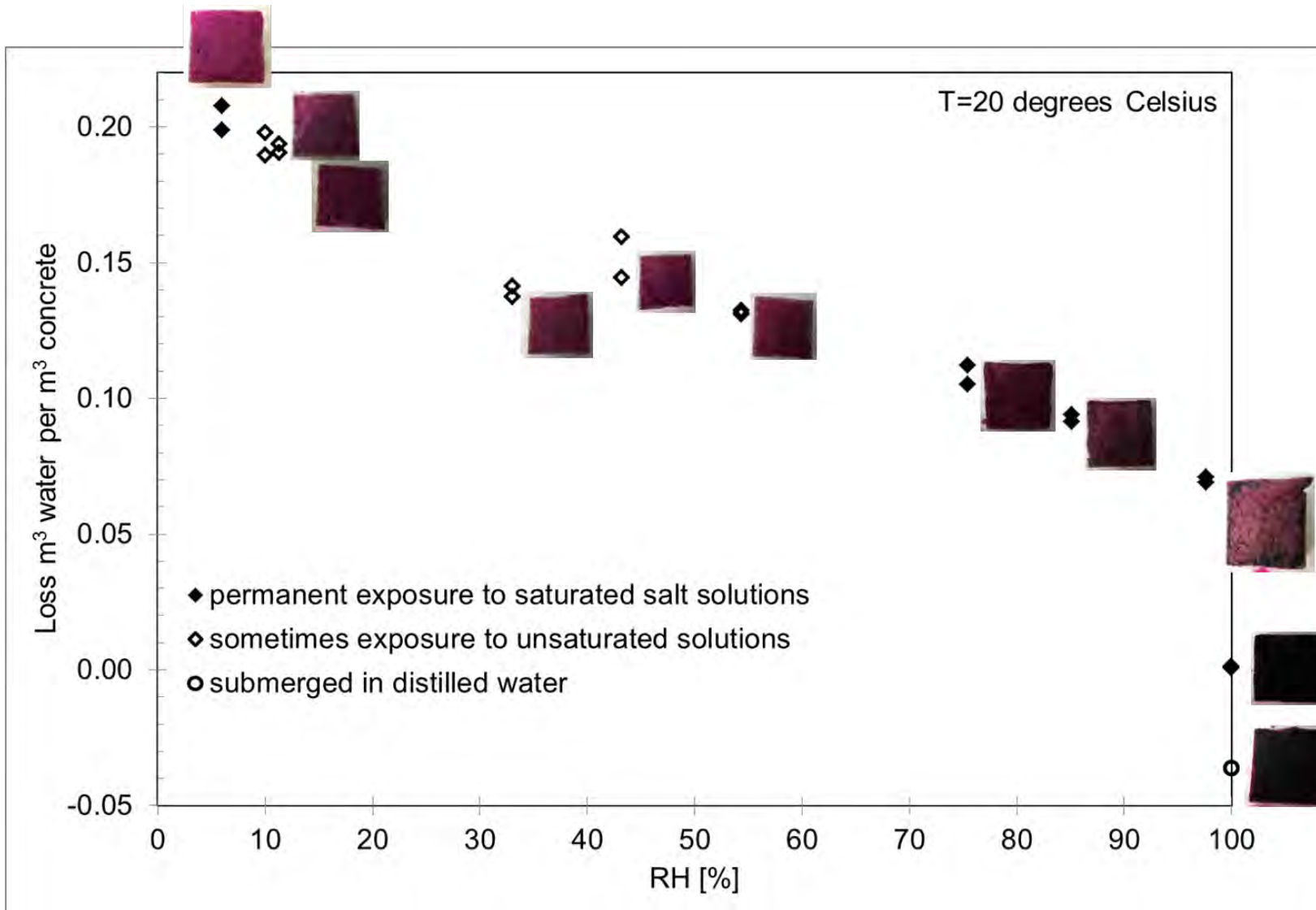


Figure 4-2: Equilibrium concentration as a function of relative humidity for backfill concrete with uncarbonated areas in purple.

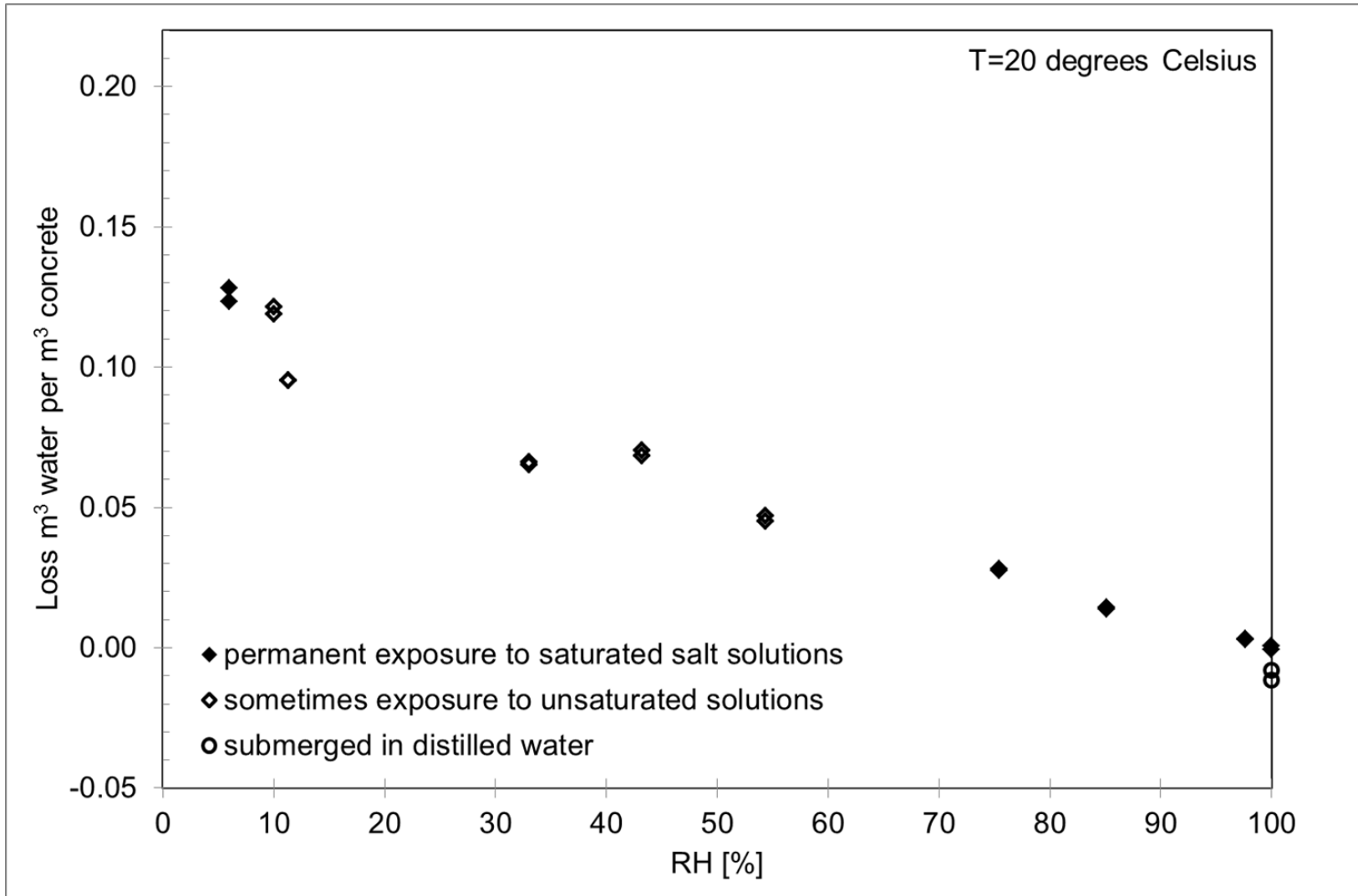


Figure 4-3: Equilibrium concentration as a function of relative humidity of buffer concrete

4.3 Exposure to clay pore water

Buffer concrete and backfill concrete have been exposed to synthetic clay pore water since 2016. Concrete samples have been put on a grid in large plastic boxes. More than 200 litres of synthetic clay pore water is present in each plastic box. The following table shows the used recipe to make clay pore water with a composition that is considered to be representative for the clay pore water in Dutch poorly indurated clay with the present available knowledge. Sand has been added in sufficient amounts to prevent under saturation of the silicon concentration.

Table 4-3: Used recipe for synthetic Dutch poorly indurated clay pore water

Solids	Gram for 1 litre clay pore water
NaCl	24.475
MgCl ₂	5.137
Na ₂ SO ₄	4.107
CaCl ₂	1.177
KCl	0.712
NaHCO ₃	0.656
KBr	0.102
H ₃ BO ₃	0.043
NaF	0.003846316
KI	0.0010
FeCl ₃	0.011139946
AlCl ₃	0.000346111

The water is kept between 16 and 20 degrees Celsius with small heating devices, some oxidation of iron occurred resulting in orange water. The following photo shows the samples that have been exposed to this synthetic clay pore water.

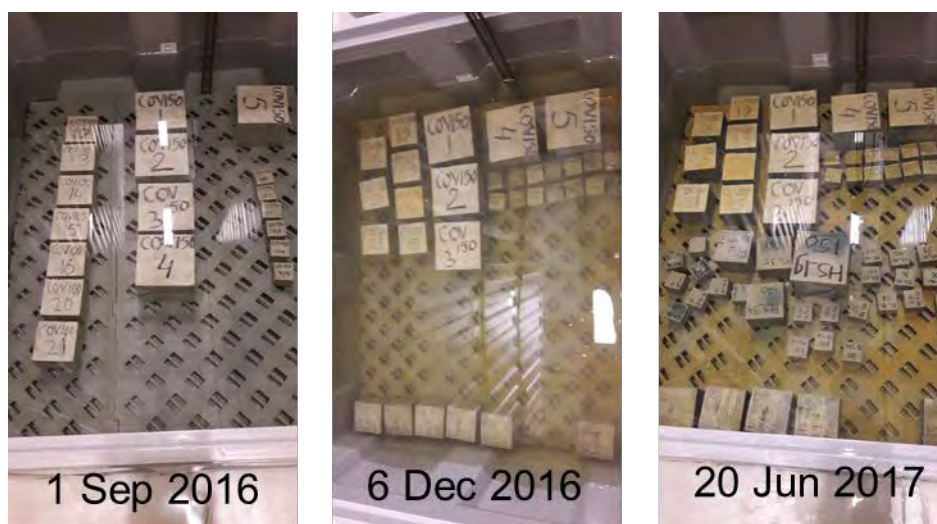


Figure 4-4: Exposure to synthetic clay pore water at several stages.

Batches of backfill concrete have been made several times in order to achieve sufficient mechanical strength and an acceptable variation in density. The batches that did not satisfy these criteria have been exposed to synthetic clay pore water since 2016 for potential future research. The recipe is similar to

backfill concrete in Table 4-2 except that they do not contain plasticiser in the concrete recipe. These batches have been made with CEM III/B as well as CEM I. Especially the ones made with CEM I may be of interest for the ASR if the investigations on the certified CEM III/B samples in Table 4-2 show no ASR and to experimentally determine the carbonation front by clay pore water exposure.



Figure 4-5: Backfill concrete samples exposed to clay pore water.

4.4 Solid characterisation

The samples will be further characterized within EURAD ACED.

The backfill concrete can be sawn by hand and that facilitates the sample preparation for all analysis to determine reaction fronts at which samples need to be taken at different positions within a concrete cubical specimen. The buffer concrete requires more sophisticated sawing to prevent artefacts as a result of the sample preparation to determine these reaction fronts.

4.4.1 ICP-OES and resistivity (COVRA)

Inductively coupled plasma mass spectrometry (ICP-OES) analysis will be performed of samples taken at different positions within a concrete cubical specimen. The measured iron content can be used to understand the transport of iron corrosion products into concrete. These measurements are expected to show how fast iron migrates in concrete as a function of the porosity and may help to understand whether cementation of iron products in concrete takes place. The ingress chlorine in concrete samples will also be measured in order to understand the measured resistivity of the samples. The resistivity will be measured in order to compare the abstracted model with experimental results. The calcium content at different positions in concrete will be measured for the samples that were submerged in distilled water as well as seawater in order to quantify leaching of calcium as a function of the chemical conditions. The calcium concentration in the concrete pore water for concrete made with CEM III/B may be almost similar to the calcium concentration in Dutch clay pore water. The leaching of cementitious components in either distilled water or seawater will first be modelled in order to judge whether ICP-OES analysis of the leached solutions will give fruitful results. Backfill concrete has an almost twice as large porosity than buffer concrete and therefore first investigated.

4.4.2 Mineralogical characterisation

Mineralogical characterization will be performed using powder XRD combined with Rietveld analyses for quantitative assessment of the phase assemblage. For the determination of the phase assemblages of the aged concrete materials by XRD, a D4 Endeavor spectrometer (Bruker AXS GmbH) with a θ - 2θ geometry or alternatively a D8 Advance (Bruker AXS GmbH) with a θ - θ geometry, both equipped with Cu X-ray tubes, will be used. Rietveld analyses will be performed using the Topas-Academic software (Version V4.1; Coelho, 2007). With respect to the Rietveld analyses, quartz aggregates will be removed from the cement paste during sample crushing and processing, to avoid that XRD spectra are dominated by quartz peaks. Moreover it is planned to investigate whether Rietveld analyses can be applied to distinguish CSH(I) and (II) in these materials. The experimental results can be compared with reactive transport modelling results in Task 3.3.

4.4.3 Aggregates (FZJ)

Microstructural investigations will be performed using SEM (e.g. in low-vacuum mode or operated as ESEM) with a field emission cathode, in particular also with respect to the potential formation of alteration rims on quartz aggregates due to ASR and evaluation of rim thickness. Elemental mappings will be performed using SEM/EDS to establish the chemical composition of hydration phases; based on the elemental mappings a segmentation technique will be applied to separate different phases/components in the concrete and for subsequent image analyses (e.g. wrt grain size of aggregates). SEM/EDS investigations will be performed using a FEI Quanta 200F SEM equipped with a field emission cathode and an Apollo X Silicon Drift Detector (SDD) from EDAX. Potential alteration rims on quartz will be investigated by RAMAN spectroscopy to get insight into the alteration mechanisms and products as well as the thickness of the altered rim zones on pristine quartz aggregates. For this purpose, a Jobin-Yvon Aramis LabRam HR Micro-Raman spectrometer (Horiba Scientific) equipped with a He-Ne laser will be used. These experimental results can be used to determine how fast ASR actually takes place. This may help to the conceptual understanding of ASR and allows comparison with the available model results in Task 3.3.

4.4.4 Other tests and characterisations

The carbonation fronts as a result of exposure to clay pore water exposure may be difficult to estimate in CEM III/B concrete samples due to the presence of trace amounts of pyrite. The discarded CEM I samples may not have this visibility problem and can be used to help to understand the carbonation by clay pore water exposure.

4.5 Interfaces with Task 2 and Task 4

4.5.1 Task 2

The steel-concrete interface is investigated in task 2. The interpretation of the iron migration in backfill concrete and buffer concrete may result in a conceptual understanding of the fate of iron as a function of porosity.

4.5.2 Task 4

Parameters for the concrete barriers can be provided i.e. porosity, diffusion values as a function of temperature and saturation degree can be provided for the model developed in Task 4. The experimental results with aggregates to investigate ASR can be used to determine when ASR needs to be included in the conceptual model. The ICP-MS analysis on the iron content and chlorine content as a function of space and exposure time can be used to validate the models in Task 4.

5 Long-term experiments on stability of cemented wastes - Gas Generation Experiment

Markku Leivo (VTT)

In many countries, low-level radioactive wastes (LLW) and intermediate-level radioactive wastes (ILW) are stored in different repositories. Other countries e.g. Finland or Switzerland store both waste sorts in one repository. In general, radioactive wastes are categorized primarily according to their radioactive inventory, which determines e.g. how to handle them until storage and over which time-scales radioactive waste sorts have to be managed. Often LLW and ILW packages are conditioned with cement materials. The degradation of organic and metallic waste, as well as the degradation of cementitious materials is normally independent from radioactive inventory and therefore it can be expected that LLW and ILW wastes evolve in a very similar way under the same storage conditions.

5.1 Test setup

In Finland low level radioactive waste (LLW) contains considerable amounts of cellulose, hemicellulose based material and metal material. Steel containers are used to store and dispose the waste. The microbial degradation of cellulose and hemicellulose, together with the utilization of hydrogen generated by metal corrosion, will result in gas generation under final repository conditions. The chemical environment inside the container and steel drums will also be strongly affected. Microbially mediated LLW degradation and gas generation processes can influence the performance of multi-barrier systems, such as by accelerating corrosion and can affect the mobility of radionuclides from the repository.

A large-scale in situ Gas Generation Experiment (GGE) was established in 1997 in Olkiluoto, Finland, to simulate the gas generation chemical changes in environment from LLW under geological repository conditions. Schematic layout of the experiment is presented in Figure 5-1. The GGE comprises sixteen 200 l carbon steel drums containing LLW from nuclear power plants at the Olkiluoto site placed within a concrete box (mass 4000 kg), as used in the VLJ repository, that is enclosed in a 20 m³ acid proof stainless steel gas tight reaction vessel. The LLW contained in the drums represents routine reactor operating waste and included cellulose (paper, cardboard, cotton), polyethylene, polyvinylchloride, polycarbonate, natural rubber, metal wastes, glass fibre and electrical components. The total masses of metal (including mild steel drums), cellulose and other organic polymers in the GGE at the start of the experiment were 379 kg, 620 kg and 596 kg respectively. The GGE tank was filled with 16m³ of locally sourced river water to provide an inoculum reflecting the plan to intentionally fill the disposal silos with water at the closure of the repository. The GGE has operated continually and largely uninterrupted from 1997 to the present day.

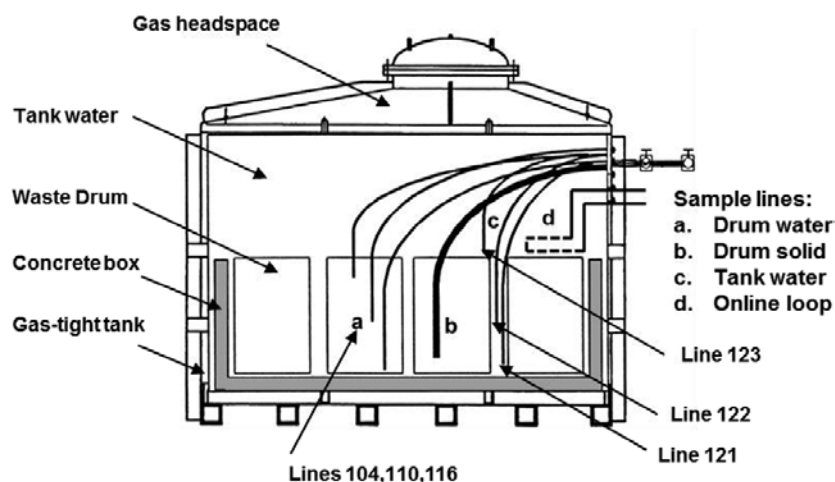


Figure 5-1: Schematic of the GGE showing different types of sampling lines (a, b, c) and online analyses (d) and location of Lines 104, 110, 116, 121, 122 and 123 that were used to take water samples. The dead volumes of the tubing are approximately 0.1–0.4 dm³. Also capsules containing a piece of drum steel and LLW were loaded to the experiment (b, drum solid). Drums are normal size 200 l steel drums (height about 0,9 m and diameter about 0,6 m). (after Small et al., 2008).

5.2 Results

Some results of the experiment are presented here. Experimental results and modelling presented in detail in Small et al. (2008), Small et.al. (2017) and Vikman et.al. (2019).

Experimental data shows that chemical conditions in various compartments of GGE tank have been very heterogeneous. During the first years of operation of the GGE, water at the drum-lid level of the tank was alkaline (pH 10–11) but pH remained close to neutral inside the drums and in the tank water at the bottom of the tank, where there is an accumulation of organic matter originating from river water (Figure 5-2). The alkalinity of the tank water has gradually declined, presumably as a result of CO₂ adsorbed into the tank water and microbial metabolites such as volatile fatty acids generated during biodegradation of LLW. The surface of the concrete is likely to have been carbonated because of the high concentrations of dissolved inorganic carbon and this may have further reduced the alkaline buffering effect of the concrete.

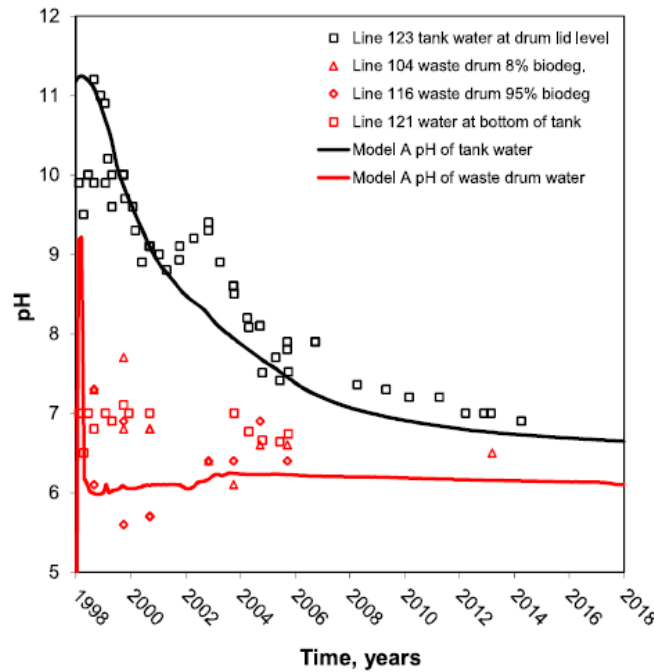


Figure 5-2: Measured pH of water samples from sample lines from the GGE and fitted average modelled pH of model cells representing tank water and waste drum regions of the experiment.

In analysing the pH of the experiment, it is assumed that the majority of the increasing Na and K concentrations in the tank water result from diffusion from the concrete box with a smaller contribution of Na and K from the waste. The majority of the Na and K measured in tank water after 18 years therefore appear to be sourced from the alkaline pore fluid present in the concrete and this fluid has a higher proportion of K than Na (Figure 5-3), again typical of cementitious leachate.

The key parameters that affect the evolution of the tank water pH in this model were found to be (i) the concentration of NaOH and KOH in the concrete (ii) the diffusion coefficients of the concrete material and (iii) the rate of enzymatic cellulose hydrolysis.

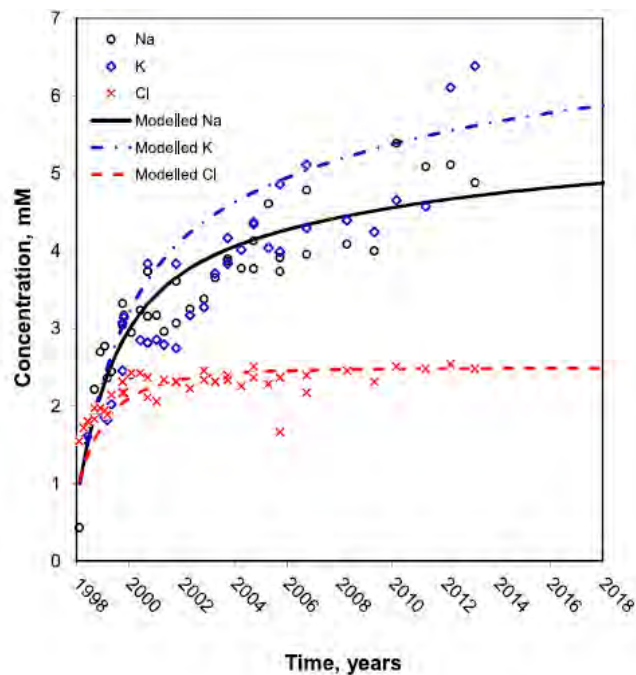


Figure 5-3: Na, K and Cl, concentration in samples of tank water.

Aqueous chemistry

Fig. 5-4 presents the concentration of S, C, Fe, Ca and Mg from samples of tank water from over the 18 years of operation of the GGE together with average modelled concentrations of the water filled region.

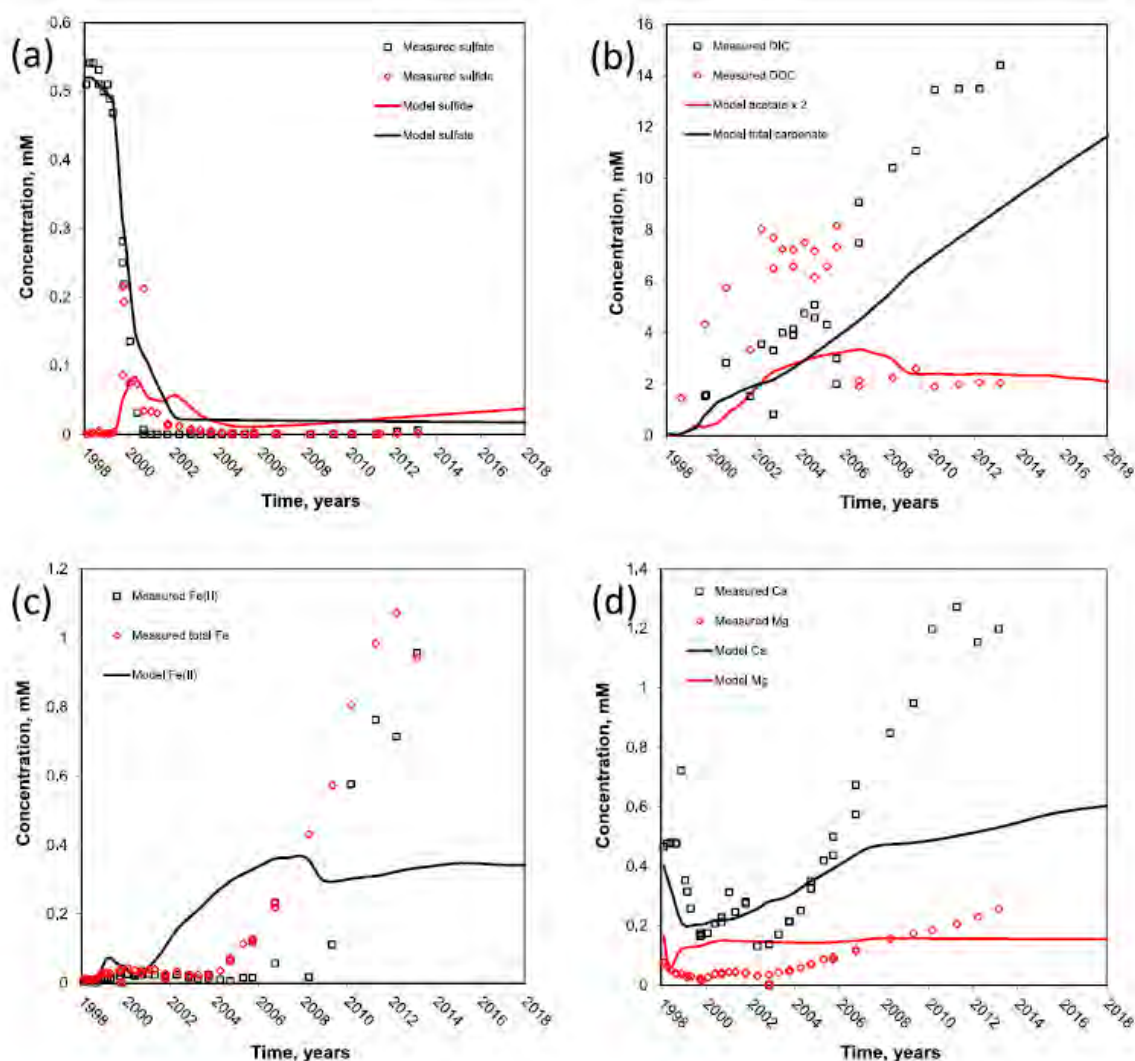


Figure 5-4: Measured concentrations of dissolved species in tank water at the drum lid level of the GGE and average modelled concentrations of tank water (a) sulphate and sulphide (b) inorganic and organic carbon (c) iron (d) calcium and magnesium. (Small et.al 2017)

Sulphate and sulphide

Sulphate reduction is clearly evident in the decline in sulphate concentration from around 0.5 mM during the first year of operation to below detection (2 µM) after September 2000 (Fig. 54a). Associated with the decline in sulphate concentration significant levels of sulphide, up to 0.2 mM, were measured during 1999 and 2000. Sulphate reduction in the tank water occurs later than observed in samples from the waste drums (Small et al., 2008). Sulphate reduction appears contemporaneous with methanogenesis within the whole of the GGE, as a result of heterogeneity between the waste and water regions.

Inorganic and organic carbon

Figure 5-4b indicates that total dissolved carbonate (DIC) concentration measured in the tank water has increased during the 18 years of operation of the experiment from below 2 mM at the start of the experiment to over 14 mM in the most recent analyses. DIC concentrations recorded from the waste drums during the first 9 years of the experiment range between 6 and 25 mM (Small et al., 2008). The

EURAD Deliverable 2.11 – ILW: Report describing the selected experiments and the existing/expected experimental results

increasing concentration of DIC in the tank water reflects the biodegradation of cellulose materials present in the waste drums that generate CO₂ in addition to CH₄.

Iron, Calcium and Magnesium

Aqueous concentrations of Fe, Ca and Mg measured in the tank water (Figure 5-4c and d) increase during the course of the experiment. The concentrations of these metals in tank water are lower than measured in the waste drums during the first 9 years of the experiment (Small et al., 2008). Both total Fe and Fe (2) had highest concentrations in a drum with high cellulose compared to the drum with relatively low cellulose content, but these are still higher than the concentrations in the tank water.

The increase in concentration of Fe, Ca and Mg observed (Figure 54c and d) are a consequence of transport of species through diffusion and mixing of water from the waste drums with the tank water. In addition, the significant lowering of the pH and increasing carbonate levels in the tank water during the 18 years of the experiment will affect Fe, Ca and Mg concentration through equilibria with mineral phases and sorption processes.

5.3 Summary

A significant observation from the GGE was that the pH conditions were heterogeneous (pH 11 to 6), providing optimal neutral pH niches for microbial activity from the outset of the experiment. Over the extended time scale of the experiment, chemical conditions were stabilized and differences in the microbial abundances and community structure in various GGE compartments became less significant. The results demonstrate that LLW is converted to methane and carbon dioxide by a succession of anaerobic processes within a complex microbial consortium. Chemical environment evolution inside the waste package is changing and it has evident implications on performance of disposal cell.

5.4 Planned work in ACED

Analyses of full-scale long-term experiment data of waste packages will be performed in ACED project by VTT. Waste package includes metal drums filled with waste placed in concrete box saturated with anoxic water. The experiment setup provides the unique possibility to use existing chemical/corrosion/gas generation data from past 21 years which may be extended by additional data acquisition within ACED. The experimental analysis will concentrate on couplings and interactions between the changes in the chemical environment provided by cementitious materials and the degradation of waste materials. It is planned to use this data in task 3.3 for calibration of long-term waste degradation, gas generation and water consumption in cemented waste packages stored in a deep geological repository

6 Concluding remarks

This deliverable intends to give a first overview of information on cemented waste (ILW) already available about existing or currently running experiments that will be studied in subtask 3.1.

A major goal of ACED is to evaluate how to pass information from relatively isolated small-scale processes investigated on interface scale to more complex systems at waste package scale and further to full disposal cell scale. In contrast to the HLW case, in most ILW disposal concepts emplacement of several or even many different waste sorts with very different waste inventory and waste package configurations in one disposal cell is planned. In order to reduce the complexity of models at disposal cell scale, it will be important to be able to get a good grip on the time scale and the spatial variability of key parameters and possible process couplings at waste package scale.

A focal point of the experimental investigations is the long term degradation of cement materials used for waste conditioning or encapsulation. This degradation might be related to contact with e.g. formation water, CO₂ produced during degradation of organic wastes, or by the use of reactive (silica) aggregates. Degradation of concrete is associated with a drop in pH. As pH affects or controls many relevant processes like degradation of organic matter and corrosion of metals the knowledge on long-term evolution of pH in a waste package will be a critical issue.

7 References

Alexander, K. M., Wardlaw, J., and Gilbert, D. J., 1968. Aggregate-Cement Bond, Cement Paste Strength and the Strength of Concrete. Proc. Conf. Structure of Concrete and Its Behaviour Under Load, London 1965, 59–92, Cement and Concrete Association, London.

Atkinson, A., Goult, D.J. and Hearne, J.A., 1985. An assessment of the long-term durability of concrete in radioactive waste repositories. MRS Online Proceedings Library Archive, 50.

Bentz, D.P. and Stutzman, P.E., 1994. Evolution of porosity and calcium hydroxide in laboratory concretes containing silica fume. Cement and Concrete Research, 24(6), pp.1044-1050.

Bernard, L. and Leemann, A., 2015. Assessing the potential of ToF-SIMS as a complementary approach to investigate cement-based materials—Applications related to alkali–silica reaction. Cement and Concrete Research, 68, pp.156-165.

Bickmore, B.R., Nagy, K.L., Gray, A.K. and Brinkerhoff, A.R., 2006. The effect of Al (OH) 4⁻ on the dissolution rate of quartz. Geochimica et Cosmochimica Acta, 70(2), pp.290-305.

Brady, P.V. and Walther, J.V., 1990. Kinetics of quartz dissolution at low temperatures. Chemical geology, 82, pp.253-264.

Chappex, T. and Scrivener, K.L., 2012. The influence of aluminium on the dissolution of amorphous silica and its relation to alkali silica reaction. Cement and Concrete Research, 42(12), pp.1645-1649.

Cheng-Yi, H. and Feldman, R.F., 1985. Hydration reactions in Portland cement-silica fume blends. Cement and Concrete Research, 15(4), pp.585-592.

Coelho, A., 2007. TOPAS Academic User Manual. Version 4.1. Coelho Software, Brisbane, Australia.

Dähn, R., Arakcheeva, A., Schaub, P., Pattison, P., Chapuis, G., Grolimund, D., Wieland, E. and Leemann, A. 2016. Application of micro X-ray diffraction to investigate the reaction products formed by the alkali-silica reaction in concrete structures. Cement and Concrete Research 79, 49-56.

Dähn, R., Popov, D., Schaub, P., Pattison, P., Grolimund, D., Mäder, U., Jenni, A. and Wieland, E. 2014. X-ray micro-diffraction studies of heterogeneous interfaces between cementitious materials and geological formations. Physics and Chemistry of the Earth 70-71, 96-103.

De Larrard, F. and Sedran, T., 1994. Optimization of ultra-high-performance concrete by the use of a packing model. Cement and Concrete Research, 24(6), pp.997-1009.

Diamond, S., Barneyback Jr, R.S. and Struble, L.J., 1981. Physics and chemistry of alkali-silica reactions (No. DOE/CS/40222-3; CONF-8103111-1). Purdue Univ., Lafayette, IN (USA);

Diamond, S., 1997. Alkali silica reactions—some paradoxes. Cement and Concrete Composites, 19(5-6), pp.391-401.

Dove, P.M. and Elston, S.F., 1992. Dissolution kinetics of quartz in sodium chloride solutions: Analysis of existing data and a rate model for 25 C. Geochimica et Cosmochimica Acta, 56(12), pp.4147-4156.

Fernandes, I., Noronha, F. and Teles, M., 2004. Microscopic analysis of alkali–aggregate reaction products in a 50-year-old concrete. Materials Characterization, 53(2-4), pp.295-306.

Glasser, F.P., 2001. Mineralogical aspects of cement in radioactive waste disposal. Mineralogical Magazine, 65(5), pp.621-633.

Glasser, F.P. 2013. Cements in Radioactive Waste Disposal (IAEA-TECDOC-CD--1701(Companion CD)). International Atomic Energy Agency (IAEA), Waste Technology Section, Vienna (Austria); Also available on: http://www-pub.iaea.org/MTCD/Publications/PDF/TE-1701_add-CD/PDF/UK%20Aberdeen%20University.pdf

Godart, B., de Rooij, M. and Wood, J. G.M., 2013. Guide for Diagnosis and Appraisal of AAR Damage to Concrete Structures, Part 1 Diagnosis (AAR 6.1) RILEM State-of-the-Art Reports, Vol. 12

EURAD Deliverable 2.11 – ILW: Report describing the selected experiments and the existing/expected experimental results

Haha, M.B., Gallucci, E., Guidoum, A. and Scrivener, K.L., 2007. Relation of expansion due to alkali silica reaction to the degree of reaction measured by SEM image analysis. *Cement and Concrete Research*, 37(8), pp.1206-1214.

Harutyunyan, V.S., Abovyan, E.S., Monteiro, P.J., Mkrтчyan, V.P., Balyan, M.K. and Aivazyan, A.P., 2003. X-ray Diffraction Investigations of Microstructure of Calcium Hydroxide Crystallites in the Interfacial Transition Zone of Concrete. *Journal of the American Ceramic Society*, 86(12), pp.2162-2166.

Ichikawa, T., 2009. Alkali–silica reaction, pessimum effects and pozzolanic effect. *Cement and Concrete Research*, 39(8), pp.716-726.

Isu, N., Ishida, H. and Mitsuda, T., 1995. Influence of quartz particle size on the chemical and mechanical properties of autoclaved aerated concrete (I) tobermorite formation. *Cement and concrete research*, 25(2), pp.243-248.

Jackson, M.D., Mulcahy, S.R., Chen, H., Li, Y., Li, Q., Cappelletti, P. and Wenk, H.R., 2017. Phillipsite and Al-tobermorite mineral cements produced through low-temperature water-rock reactions in Roman marine concrete. *American Mineralogist*, 102(7), pp.1435-1450.

Jacques, D., Maes, N., Perko, J., Seetharam, S.C., Phung, Q.T., Patel, R., Soto, A., Liu, S., Wang, L., De Schutter, G. and Ye, G., 2014, February. Concrete in Engineered Barriers for Radioactive Waste Disposal Facilities: Phenomenological Study and Assessment of Long Term Performance. In ASME 2013 15th International Conference on Environmental Remediation and Radioactive Waste Management. American Society of Mechanical Engineers Digital Collection.

Jacques, D., Dauzères, A., Deissmann, G., Govaerts, J., Holt, E., Kosakowski, G., Leivo, M., Martin C., and Neeft, E., 2019. EURAD ACED - Assessment of Chemical Evolution of ILW and HLW Disposal Cells. Euradwaste ' 19 European Commission conference on EURATOM Research and Training in Radioactive Waste Management, 4-7 June 2019, Pitesti, Romania.

Jensen V 1993. Alkali Aggregate Reaction in Southern Norway, doctoral thesis, Technical University of Trondheim, NTH, Norway: pp 265 +10 Appendices

Kořátková, J., Zatloukal, J., Reiterman, P. and Kolář, K., 2017. Concrete and cement composites used for radioactive waste deposition. *Journal of environmental radioactivity*, 178, pp.147-155.

Leemann, A., 2017. Raman microscopy of alkali-silica reaction (ASR) products formed in concrete. *Cement and Concrete Research*, 102, pp.41-47.

Leemann, A. and Münch, B., 2019. The addition of caesium to concrete with alkali-silica reaction: Implications on product identification and recognition of the reaction sequence. *Cement and Concrete Research*, 120, pp.27-35.

Leupin, O.X., Smith, P., Marschall, P., Johnson, L., Savage, D., Cloet, V., Schneider, J., and Senger, R., 2016. Low- and intermediate-level waste repository-induced effects. Nagra Technical Report 14-14. Nagra, Wettingen, Switzerland.

Lindgård, J., Andiç-Çakır, Ö., Fernandes, I., Rønning, T.F. and Thomas, M.D., 2012. Alkali–silica reactions (ASR): Literature review on parameters influencing laboratory performance testing. *Cement and concrete research*, 42(2), pp.223-243.

Lothenbach, B., Le Saout, G., Gallucci, E. and Scrivener, K., 2008. Influence of limestone on the hydration of Portland cements. *Cement and Concrete Research*, 38(6), pp.848-860.

Lothenbach, B., Scrivener, K. and Hooton, R.D., 2011. Supplementary cementitious materials. *Cement and concrete research*, 41(12), pp.1244-1256.

Lothenbach, B., Winnefeld, F., Alder, C., Wieland, E. and Lunk, P., 2007. Effect of temperature on the pore solution, microstructure and hydration products of Portland cement pastes. *Cement and Concrete Research*, 37(4), pp.483-491.

EURAD Deliverable 2.11 – ILW: Report describing the selected experiments and the existing/expected experimental results

Malinowski, R., 1979. Concretes and mortars in ancient aque-ducts. *Concrete International*, 1(1), pp.66-76.

Mazloom, M., Ramezani-pour, A.A. and Brooks, J.J., 2004. Effect of silica fume on mechanical properties of high-strength concrete. *Cement and Concrete Composites*, 26(4), pp.347-357.

Mazurek M, Gautschi A, Marschall P, Vigneron G, Lebon P, 2008. Transferability of geoscientific information from various sources (study sites, underground laboratories, natural analogues) to support safety cases for radioactive waste repository in argillaceous formations, *Physics and Chemistry of the Earth*, S95-S105.

Mehta, K.P., 2001. Reducing the environmental impact of concrete. *Concrete international*, 23(10), pp.61-66.

Mehta, P.K., Monteiro, P.J.M., 2014. *Concrete: Microstructure, Properties, and Materials*, 4th ed., McGraw-Hill Companies, New York City.

Mitsuda, T., Sasaki, K. and Ishida, H., 1992. Phase evolution during autoclaving process of aerated concrete. *Journal of the American Ceramic Society*, 75(7), pp.1858-1863.

Monteiro, P.J.M. and Mehta, P.K., 1986. Interaction between carbonate rock and cement paste. *Cement and Concrete Research*, 16(2), pp.127-134.

Moropoulou, A., Bakolas, A. and Anagnostopoulou, S., 2005. Composite materials in ancient structures. *Cement and concrete composites*, 27(2), pp.295-300.

Okada, K., Nishibayashi, S. and Kawamura, M., 2004. *Alkali-aggregate Reaction: 8th International Conference*. CRC Press.

Ollivier, J.P., Maso, J.C. and Bourdette, B., 1995. Interfacial transition zone in concrete. *Advanced cement based materials*, 2(1), pp.30-38.

Poole, A.B. and Sims, I., 2015. *Concrete petrography: a handbook of investigative techniques*. Crc Press.

Poon, C.S., Kou, S.C. and Lam, L., 2006. Compressive strength, chloride diffusivity and pore structure of high performance metakaolin and silica fume concrete. *Construction and building materials*, 20(10), pp.858-865.

Poyet, S., 2009. Experimental investigation of the effect of temperature on the first desorption isotherm of concrete. *Cement and Concrete Research*, 39(11), pp.1052-1059.

Rajabipour, F., Giannini, E., Dunant, C., Ideker, J.H. and Thomas, M.D., 2015. Alkali–silica reaction: current understanding of the reaction mechanisms and the knowledge gaps. *Cement and Concrete Research*, 76, pp.130-146.

RILEM TC 106-AAR, 'Alkali aggregate reaction'. TC 106-2—Detection of potential alkali-reactivity of aggregates—the ultra-accelerated mortar-bar test B. TC106-3—Detection of potential alkali-reactivity of aggregates—method for aggregate combinations using concrete prisms, *Mater. Struct.* 33 (2000) 283–293.

RILEM TC 191-ARP, 'Alkali-reactivity and prevention—assessment, specification and diagnosis of alkali-reactivity', RILEM recommended test method AAR-1: detection of potential alkali-reactivity of aggregates—petrographic method, *Materials and Structures* 36 (2003) 480–496.

Scrivener, K.L., Crumby, A.K. and Laugesen, P., 2004. The interfacial transition zone (ITZ) between cement paste and aggregate in concrete. *Interface science*, 12(4), pp.411-421.

Shi, Z., Geng, G., Leemann, A. and Lothenbach, B., 2019. Synthesis, characterization, and water uptake property of alkali-silica reaction products. *Cement and Concrete Research*, 121, pp.58-71.

EURAD Deliverable 2.11 – ILW: Report describing the selected experiments and the existing/expected experimental results

Silva, D.A., Wenk, H.R. and Monteiro, P.J.M., 2005. Comparative investigation of mortars from Roman Colosseum and cistern. *Thermochimica Acta*, 438(1-2), pp.35-40.

Small, J., Nykyri, M., Helin, M., Hovi, U., Sarlin, T., Itävaara, M., 2008. Experimental and modelling investigations of the biogeochemistry of gas production from low and intermediate level radioactive waste. *Applied Geochemistry* 23, 1383–1418.

Small, J., Nykyri, M., Vikman, M., Itävaara, M. & Heikinheimo, L. 2017. The biogeochemistry of gas generation from low-level nuclear waste: Modelling after 18 years study under in situ conditions. *Applied Geochemistry* 84, 360e372.

Swamy, R.N. ed., 2002. *The alkali-silica reaction in concrete*. CRC Press.

Tasong, W.A., Cripps, J.C. and Lynsdale, C.J., 1998. Aggregate-cement chemical interactions. *Cement and Concrete Research*, 28(7), pp.1037-1048.

Tasong, W.A., Lynsdale, C.J. and Cripps, J.C., 1999. Aggregate-cement paste interface: Part I. Influence of aggregate geochemistry. *Cement and Concrete Research*, 29(7), pp.1019-1025.

Vikman, M., Marjamaa, K., Nykyri, M., Small, J., Miettinen, H., Heikinheimo, L., Haavisto, T. and Itävaara, M., 2019. The biogeochemistry of gas generation from low-level nuclear waste: Microbiological characterization during 18 years study under in situ conditions. *Applied Geochemistry* 105, 55–67

Yazıcı, H., Deniz, E. and Baradan, B., 2013. The effect of autoclave pressure, temperature and duration time on mechanical properties of reactive powder concrete. *Construction and Building Materials*, 42, pp.53-63.

Yuan, C.Z. and Odler, I., 1987. The interfacial zone between marble and tricalcium silicate paste. *Cement and Concrete Research*, 17(5), pp.784-792.